



HAL
open science

Experimental and Modeling Investigation of the Low-Temperature Oxidation of Dimethyl Ether

Anne Rodriguez, Ophélie Frottier, Olivier Herbinet, René Fournet, Roda Bounaceur, Christa Fittschen, Frédérique Battin-Leclerc

► **To cite this version:**

Anne Rodriguez, Ophélie Frottier, Olivier Herbinet, René Fournet, Roda Bounaceur, et al.. Experimental and Modeling Investigation of the Low-Temperature Oxidation of Dimethyl Ether. *Journal of Physical Chemistry A*, 2015, 119, pp.7905-7923. 10.1021/acs.jpca.5b01939 . hal-01178238

HAL Id: hal-01178238

<https://hal.science/hal-01178238v1>

Submitted on 17 Jul 2015

HAL is a multi-disciplinary open access archive for the deposit and dissemination of scientific research documents, whether they are published or not. The documents may come from teaching and research institutions in France or abroad, or from public or private research centers.

L'archive ouverte pluridisciplinaire **HAL**, est destinée au dépôt et à la diffusion de documents scientifiques de niveau recherche, publiés ou non, émanant des établissements d'enseignement et de recherche français ou étrangers, des laboratoires publics ou privés.

Experimental and modeling investigation of the low-temperature oxidation of dimethylether

Anne Rodriguez¹, Ophélie Frottier¹, Olivier Herbinet¹, René Fournet¹, Roda Bounaceur¹,
Christa Fittschen², Frédérique Battin-Leclerc^{1*}

¹*Laboratoire Réactions et Génie des Procédés, CNRS, Université de Lorraine, BP 20451,
1 rue Grandville, 54000 Nancy, France*

²*PhysicoChimie des Processus de Combustion et de l'Atmosphère, CNRS, Université de Lille 1,
59650 Villeneuve d'Ascq, France*

Abstract

The oxidation of dimethylether (DME) was studied using a jet-stirred reactor over a wide range of conditions: temperatures from 500 to 1100 K, equivalence ratios of 0.25, 1 and 2, residence time of 2 s, pressure of 106.7 kPa (close to the atmospheric pressure) and an inlet fuel mole fraction of 0.02 (with high dilution in helium). Reaction products were quantified using two analysis methods: gas chromatography and continuous wave cavity ring down spectroscopy (cw-CRDS). cw-CRDS enabled the quantification of formaldehyde which is one of the major product from DME oxidation as well as that of hydrogen peroxide which is an important branching agent in low-temperature oxidation chemistry. Experimental data were compared with data computed using models from the literature with important deviations being observed for the reactivity at low-temperature. A new detailed kinetic model for the oxidation of DME was developed in this study. Kinetic parameters used in this model were taken from literature or calculated in the present work using quantum calculations. This new model enables a better prediction of the reactivity in the low-temperature region. Under the present JSR conditions, error bar on predictions were given. Simulations were also successfully compared with experimental flow reactor, jet-stirred reactor, shock tube, rapid compression machine and flame data from literature. The kinetic analysis of the model enabled to highlight some specificities of the oxidation chemistry of DME: 1) the early reactivity which is observed at very low-temperature (e.g., compared to propane) is explained by the absence of inhibiting reaction of the radical directly obtained from the fuel (by H-atom abstraction) with oxygen yielding an olefin + HO₂•; 2) the low-temperature reactivity is driven by the relative importance of the second addition to O₂ (promoting the reactivity through branching chain) and the competitive decomposition reactions with an inhibiting effect.

Keywords: dimethylether; oxidation; jet-stirred reactor; modeling; quantum calculation; cw-CRDS.

* Corresponding author: frederique.battin-leclerc@univ-lorraine.fr

Introduction

Dimethylether (DME, CH_3OCH_3) is a synthetic gaseous (under standard conditions) fuel which can be produced from a wide range of feed-stocks such as natural gas [1], coal [2], black liquor [3] or biomass [4] though the dehydrogenation of methanol obtained from syngas [5]. With its high cetane number (>55) and its lower autoignition temperature compared to diesel fuel, DME is considered as a potential ultra-clean replacement fuel [6], for being used in blend with diesel fuel in compression-ignition engines, with also a potential reduction of soot formation [1].

There are a particularly large number of kinetic studies about the combustion and oxidation of DME. Table 1 presents recent experimental studies performed in jet-stirred reactors, flow tubes, shock tubes, rapid compression machines, burners, and spherical bombs for the oxidation of this linear ether.

As shown by Table 1, the autoignition of DME has been mostly studied in flow tubes, with the earliest studies made in 1999-2001 [7–10] and then new ones performed from 2013. These studies well concerned low-temperature oxidation since they have all been performed at temperatures below 800 K. The most recent studies have been performed in Bielefeld [11–13] and in Princeton [14–16] using mainly molecular beam mass spectrometry detection method. The specificity of the work made in Princeton concerns the detection of high amounts of H_2O_2 [14,16], an intermediate which is rarely analyzed but is crucial in the low-temperature oxidation chemistry of organic fuels [17]. Many studies were also performed using shock tubes, with the earliest work performed by Pfahl et al. in 1996 [18] at temperature starting from 630 K, i.e. in a range where low-temperature chemistry is of importance. This is also the case of the most recent study of Li et al. in 2013 [19]. The temperatures investigated during the other studies are in a higher range (i.e. from 950 K and above). Recently Lynch et al. [20] used a miniature shock tube with synchrotron VUV photo ionization mass spectrometry to study the pyrolysis of DME. Two studies [21,22] about ignition were also performed in rapid compression machines. DME flame structures were studied using low-pressure or atmospheric premixed flames [23–28] with species quantification performed using molecular beam mass spectrometry. Laminar burning velocities were measured using burners [29,30] or spherical bombs [31–35]. Only two studies of the low-temperature oxidation of DME have been performed in a jet-stirred reactor. The first one, in 1998, used gas chromatography (GC) as detection method to analyze reaction products containing up to 2 heavy atoms [36,37]. The second study was very recently performed and used mass spectrometry with synchrotron radiation for the detection of the aldo-hydroperoxide (hydroperoxymethyl formate) formed during the low-temperature oxidation of DME at 540 K. This last species cannot be observed using gas chromatography [38]. Other important intermediates identified during this study were formaldehyde, hydrogen peroxide, formic acid, methyl hydroperoxide, 1,3-dioxetane and methyl formate. Mass spectra and photoionization efficiency curves were provided, but no product quantification were given.

Besides the different models which have been proposed to reproduce results obtained in one or two of the experimental devices listed in Table 1 (e.g., [9,36]), two recent models aimed at modeling a wide range of experimental data: that of Zhao et al. written in 2008 [39] and that just published by Burke et al. [22]. These two models present validations for low-temperature oxidation and ignition, but also for pyrolysis and flames.

The purpose of this paper is to present a new experimental and modeling study of the low-temperature oxidation of DME based on an experimental work performed in a jet-stirred reactor using GC and continuous wave cavity ring-down spectroscopy (cw-CRDS) as detection methods for a comprehensive quantification of reaction products. GC was used to analyze reaction products containing up to 3 heavy atoms. In line with our recent work on *n*-butane oxidation [17], cw-CRDS was used for the quantification of H₂O, CH₂O and H₂O₂. The present study is the first to propose the quantification of H₂O₂, a very important intermediate in combustion phenomena, during the oxidation of DME in a jet-stirred reactor. This paper also presents a new detailed kinetic model developed based on a theoretical investigation of the reactions involving CH₃OCH₂OO• and derived radicals and validated using mainly data obtained for low-temperature oxidation and ignition, but with also a few tests for pyrolysis and flame. A comparison of present experimental data with data computed with literature models is proposed. Large differences in the reactivity, especially observed at low temperature, have justified the development of the new detailed kinetic model presented in this paper.

Table 1: Recent experimental studies performed in jet-stirred reactors, flow tubes, shock tubes, rapid compression machines, burners and spherical bombs for the oxidation of dimethylether.

Type of experiments	Experimental conditions	References
Jet-stirred reactor	T = 800-1300K ; P = 101-1013kPa ; ϕ = 0.2-2 ; τ = 0.1s	Dagaut et al. 1996 [36]
	T = 550-1100K ; P = 1013kPa ; ϕ = 0.2-1 ; τ = 0.1s	Dagaut et al. 1998 [37]
	T = 540K ; P = 976kPa ; ϕ = 0.35 ; τ = 5s	Moshhammer et al. 2015 [38]
Flow tube	T = 600-1500K ; P = 101kPa ; ϕ = 0.5	Alzueta et al. 1999 [7]
	T = 1080-1086K ; 101kPa ; ϕ = 0.5 ; τ = 0.1s	Fischer et al. 2000 [8]
	T = 550-855K ; P = 1216-1824kPa ; ϕ = 0.7-4.2 ; τ = 1.8s	Curran et al. 2000 [9]
	T = 513-973K ; P = 101kPa ; 340 ppm in 10% O ₂ ; τ = 2-4s	Liu et al. 2001 [10]
	T = 490-750K ; τ = 107s ; ϕ = 0.6	Guo et al. 2013 [14]
	T = 623K ; P = 101kPa ; ϕ = 0.3 ; τ = 0.35s	Brumfield et al. 2013 [15]
	T = 500-1200K ; P = 101kPa ; ϕ = 0.8-1.2	Herrmann et al. 2013 [11], 2014 [12]
Shock tube	T = 500-1150K ; P = 101kPa ; ϕ = 0.2-1.6 ; τ = 0.19-2s	Kurimoto et al. 2015 [16]
	T = 500-1150K ; P = 101kPa ; ϕ = 1 ; τ = 1.5s	Wang et al. [13]
	T = 650-1300K ; P = 1317-4053kPa ; ϕ = 1	Pfahl et al. 1996 [18]
	T = 1200-1600K ; P = 350kPa ; ϕ = 0.5-2	Dagaut et al. 1998 [37]
	T = 1175-1900K ; P = 161-666kPa ; ϕ = 0.5-3	Cook et al. 2009 [40]
	T = 1134-2015K ; P = 101-1010kPa ; ϕ = 1	Tang et al. 2012 [41]
	T = 697-1239K ; P = 2200-2300kPa ; ϕ = 0.5-1.5	Li et al. 2013 [19]
T = 400-1160K ; P = 1111-3030kPa ; ϕ = 0.3-2	Burke et al. 2014 [22]	
T = 1400-1700K ; P = 300-1600kPa ; <i>pyrolysis</i>	Lynch et al. 2015 [20]	
Rapid compression machine	T = 615-735K ; P = 1010-2010kPa ; ϕ = 0.43-1	Mittal et al. 2012 [21]
	T = 630-1250K ; P = 1111-3030kPa ; ϕ = 0.3-2	Burke et al. 2014 [22]

Table 1 (continued).

Type of experiments	Experimental conditions	References
Burner	Premixed flame ^a , P = 4kPa ; $\varphi = 0.98-1.20$	Mcilroy et al. 2000 [23]
	Premixed flame ^a , atmospheric pressure ; $\varphi = 0.67-1.49$	Kaiser et al. 2000 [24]
	Premixed flame ^a , P = 2.67-4kPa ; $\varphi = 1.2-1.68$	Cool et al. 2007 [25]
	Premixed flame ^a , P = 4kPa ; $\varphi = 0.5-2.0$	Wang et al. 2008 [26]
	Premixed flame ^a , P = 4kPa ; $\varphi = 1$	Xu et al. 2011 [27]
	Premixed flame ^a , P = 5kPa ; $\varphi = 1.63$	Liu et al. 2013 [28]
	Single jet-wall stagnation flame ^b , atmospheric pressure, T = 298 K, $\varphi = 0.7-1.7$	Zhao et al. 2004 [29]
	Counterflow flame ^b , atmospheric pressure, room temperature, $\varphi = 0.7-1.7$	Wang et al. 2009 [30]
Spherical bomb ^b	P = 100kPa, T = 295 K, $\varphi = 0.7-1.7$	Daly et al. 2001 [31]
	P = 200-1000kPa, room temperature, $\varphi = 0.6-1.7$	Qin and Ju 2005 [32]
	P = 80 -150kPa, T = 285 K, $\varphi = 0.7-1.8$	Huang et al. 2007 [33]
	P = 97kPa, T = 293K, $\varphi = 0.7-1.8$	Chen et al. 2009 [34]
	P = 100-1000kPa, T = 298K, $\varphi = 0.7-1.6$	de Vries et al. 2011 [35]

^a: For species profile measurements, ^b: For laminar burning velocity measurement.

Experimental procedure

DME oxidation experiments were performed using a fused silica jet-stirred reactor (JSR) which has already been used for numerous gas phase oxidation studies and has been described in previous papers [42–44]. This is a continuous flow reactor operated at steady state with constant temperature, pressure and gas flow rate.

Several diagnostics were used for the quantification of reaction products: gas chromatography and cw-CRDS (continuous-wave cavity ring-down spectroscopy). Two gas chromatographs were needed for the quantification of the range of products from methane up to C₃ species. The first one was equipped with a carbosphere packed column and a thermal conductivity detector. It was used for the quantification of O₂, CO and CO₂, with a detection limit of about 100 ppm. Despite disadvantageous conditions (use of helium as carrier gas, a gas with a close thermal conductivity compared to hydrogen), hydrogen was detected during some experiments (at an equivalence ratio of 1 in the high temperature region) but could not be quantified due to very low signals.

The second gas chromatograph was equipped with a PlotQ capillary column and a flame ionization detector for the quantification of C₁-C₃ species. The flame ionization detector was preceded by a methanizer enabling the detection of species containing carbonyl functions with a better sensitivity (detection limit in the range 1-10 ppm depending on species). Note that the detection of formaldehyde by gas chromatography was possible but that the uncertainty in mole fractions is relatively high (estimated to ±20%, compared to ± 5% for other species) due to very tailing peaks in chromatograms and coelution. Formaldehyde could be quantified with a better accuracy using cw-CRDS. Another gas chromatograph equipped with a PlotQ capillary column and coupled to a mass spectrometer (with electron impact at 70 eV) was used for the identification of species.

Calibrations of gas chromatographs were performed by injected gaseous standards provided by Messer. Uncertainties in mole fraction were estimated to ± 5% for these species (this estimation was obtained by performing repeatability tests). Note that uncertainties in fuel mole fractions are larger (about ± 20%) because this oxygenated compound tends to adsorb on surfaces during the transfer from the reactor to gas chromatographs.

Continuous wave cavity ring down spectroscopy (cw-CRDS) is a technique which relies on the absorption of species: in the present work the near infrared range (6620-6644 cm⁻¹) has been considered. This technique was already successfully used for the detection of several species formed in the oxidation of methane and *n*-butane in a jet-stirred reactor [45,17,46]. In the present study, cw-CRDS was used for the quantification of water, formaldehyde and hydrogen peroxide. The measurement cell is composed of a glass tube with a cavity formed by two highly reflective mirrors fixed at each extremity of the cell. One of the two mirrors is fixed to a piezo actuator enabling the periodic modulation of the cavity length in order to obtain resonance between the wavelength and the cavity modes. A diode laser beam enters the cell through one mirror and the signal exiting through the other mirror after many round trips was recorded using an avalanche photo-diode. When the cavity length comes into resonance with the laser light, the recorded signal increases and exceeds a user defined threshold. At this moment, a homemade threshold circuit triggers an acousto-optical modulator and the laser beam was deviated. The decay signal was subsequently recorded as a function

of time and the ring-down time is obtained by fitting the exponential decay over a time range of seven lifetimes by a Levenberg-Marquardt exponential fit [45]. 50 ring-down events are typically averaged before incrementing the wavelength of the diode by 0.03 cm^{-1} . **Erreur ! Source du renvoi introuvable.** displays the absorption spectrum obtained during an oxidation experiment of DME at 625 K as well as spectra for neat water, hydrogen peroxide/water mixture and formaldehyde. Lines used for the quantification are identified with a "*" symbol. Absorption lines and cross sections used for the quantification are given in Table 2.

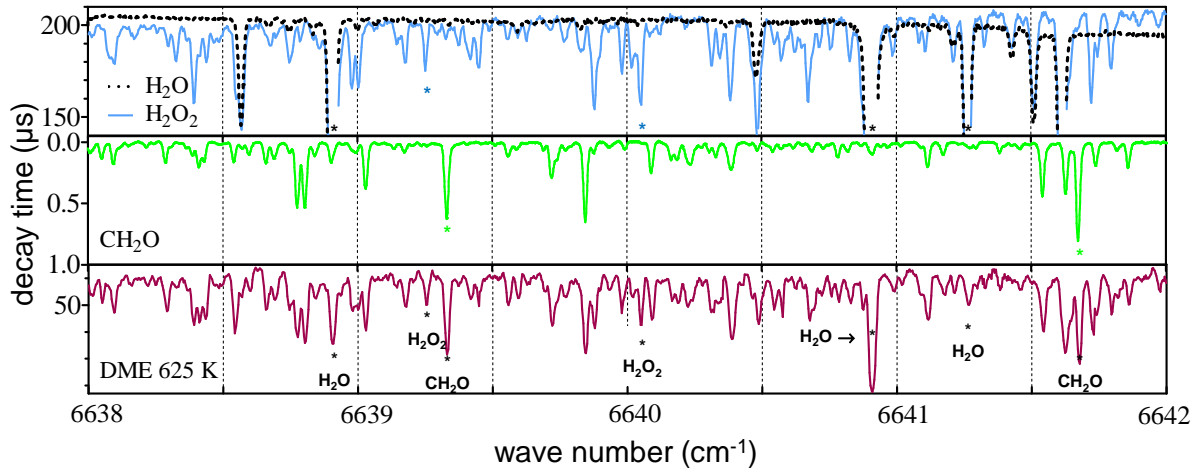


Figure 1: Comparison of an absorption spectrum measured during a DME oxidation experiment at 625 K (lower panel) and reference spectra for neat H_2O , H_2O_2 and CH_2O . "*" in panels indicate absorption lines used for the quantification (see Table 2).

Table 2: Absorption lines and cross sections used for the quantification of formaldehyde, water and hydrogen peroxide.

	wavenumber ν (cm^{-1})	cross section σ (cm^2)	reference
CH_2O	6639.33	3.60×10^{-22}	Morajkar et al. [47]
	6641.67	4.59×10^{-22}	
H_2O	6638.9*	4.46×10^{-23}	Macko et al. [48]
	6640.9	1.60×10^{-22}	
	6641.27*	1.82×10^{-22}	
H_2O_2	6639.26	7.62×10^{-23}	Parker et al. [49]
	6640.06	1.41×10^{-22}	

* These lines were used only at high temperature because they were perturbed by another peak at low-temperature resulting in uncertainties.

Mole fractions were calculated using two different absorption lines for each species to check the consistency of the data. The line at 6641.67 cm^{-1} for formaldehyde was used at low temperature only because at high temperature this line is too close to one line for H_2O . Note that uncertainties in mole fractions are mainly due to uncertainties in cross sections and in measured ring down times. The average uncertainty in mole fractions was estimated to an average of $\pm 15\%$ depending on the absorption line and the species concentration. The uncertainties in water mole fractions are larger at

high temperatures due to the huge concentration of this species in the cell which eventually leads to line saturation above 850 K. The detection limit depends on the intensity of the absorption line (about 500 ppm here).

Atom balances have been checked by comparing numbers of carbon, oxygen and hydrogen atoms at the inlet and at the outlet of the reactor. Globally these atom balances are satisfactory given the uncertainties in mole fractions (e.g., $\pm 20\%$ for some important products like CH_2O and H_2O). Carbon atom balances are around 100% at any temperature at $\varphi = 0.25$. They are around 100% up to 850 K at $\varphi = 1$. Above this temperature the carbon atom balance progressively deteriorates down to 50 % likely due to heavy compounds which were not quantified. The same phenomena is observed at $\varphi = 2$. As far as oxygen atom balances are concerned, they are around 100% at any temperature at $\varphi = 0.25$ and at temperatures up to 850 K at other equivalence ratios. Above 850 K they are around 125 %. This could be due to uncertainties in water which is formed in large concentrations in this temperature zone. Hydrogen atom balances are around 100% at all equivalence ratios below 850 K. Above this temperature, they are around 130 % at $\varphi = 0.25$, around 120% at $\varphi = 1$ and progressively decrease down to 65% at $\varphi = 2$. Again this could be related to uncertainties in water mole fractions. Note that hydrogen, which is likely an important intermediate formed under rich conditions) could not be quantified in this study which can explain the observed decreasing trend, especially at $\varphi = 2$.

Experimental results

Jet-stirred reactor experiments have been performed at temperatures ranging from 500 to 1100 K, a pressure of 106.7 kPa, a residence time of 2 s, a fuel inlet mole fraction of 0.02 and three equivalence ratios (0.25, 1 and 2) with dilution in helium.

The evolution of the mole fraction of the reactants with temperature is displayed in Figure 2 (for clarity, experimental error bars are plotted for the stoichiometric mixture experiments only). One particularity of DME, which can be spotted in Figure 2, is that the start of reactivity is observed from 525 K. This is unusual for such a small molecule. In comparison, the start of reactivity was observed for propane oxidation at low-temperature in an atmospheric pressure jet-stirred reactor only from 600 K, although conditions were more favorable (longer residence time of 6 s and much larger inlet fuel mole fraction of 0.12) [50]. The reason for the larger reactivity of DME will be explained in the discussion part of this paper.

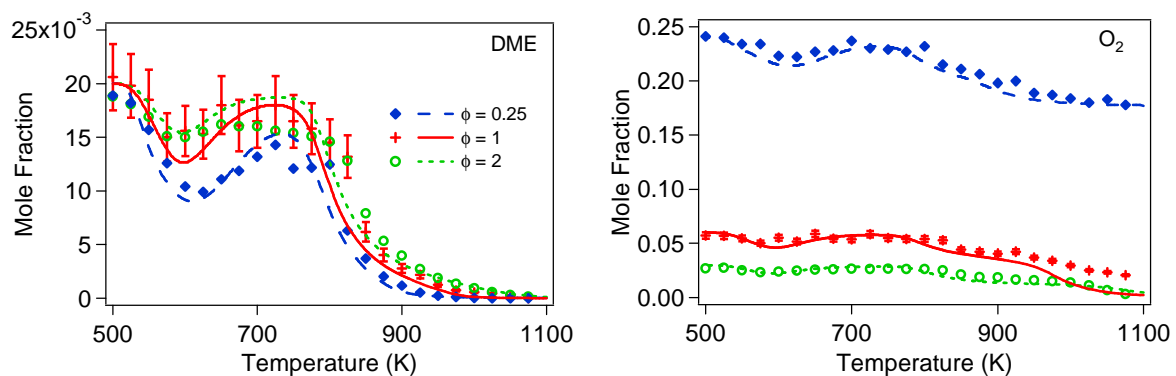


Figure 2 : Mole fractions of DME and O₂ ($x_{fuel} = 0.02$, $P = 106.7$ kPa, $\tau = 2$ s, $\phi = 0.25, 1$ & 2). Symbols represent experimental data and lines the simulations using the present model. Experimental error bars are only shown for $\phi = 1$.

The reactivity profiles are very similar for the rich and stoichiometric mixtures with a maximum conversion of about 25 % at 600 K and a very small negative temperature coefficient behavior (the conversion does not return to zero in the transition region). The equivalence ratio has a more significant effect on the reactivity in the lean mixture in the low temperature region with a maximum conversion of about 50 % at 625 K. Again a negative temperature coefficient area is observed with a minimum conversion of about 25 % in the transition region, confirming the highly reactive nature of this fuel.

The species quantified by gas chromatography are displayed in Figure 2 to Figure 4. These species are hydrocarbons (methane, acetylene, ethylene, ethane, propene and propane, in Figure 3) and oxygenated compounds (CO, CO₂, formaldehyde, acetaldehyde and methyl-formate, in Figure 4). Hydrogen was only detected at $\phi=1$ in the high temperature region but was not quantified due to very low signals. Species quantified using cw-CRDS are water, formaldehyde and H₂O₂. Formic acid, which was detected during some flow tube experiments [8,9,16] and during recent JSR experiments [38], was not detected in this study (even using gas chromatography coupled to mass spectrometry). This is likely due to low concentrations of this species.

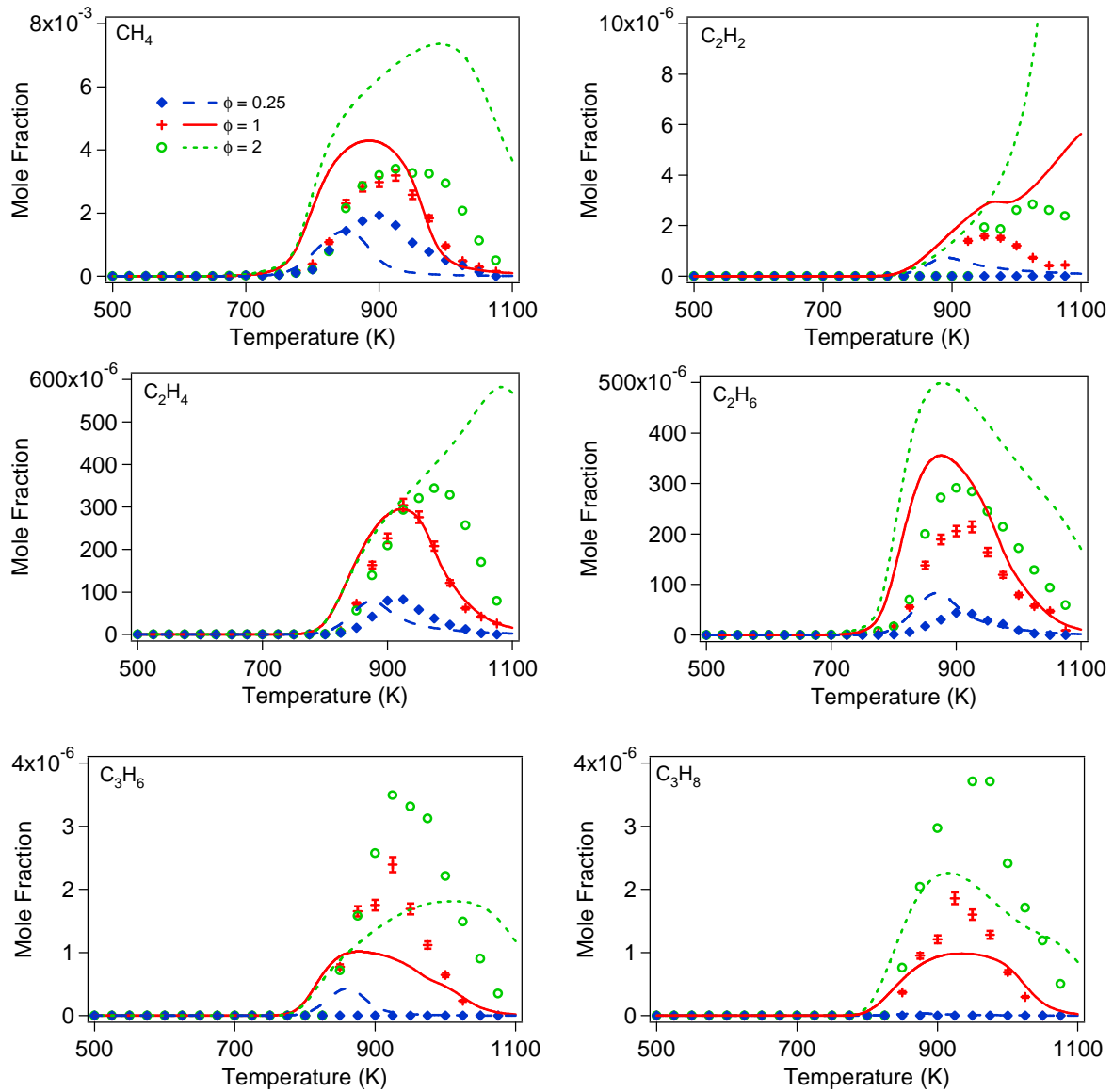


Figure 3 : Mole fractions of hydrocarbon reaction products ($x_{fuel} = 0.02$, $P = 106.7$ kPa, $\tau = 2$ s, $\phi = 0.25, 1$ & 2). Symbols represent experimental data and lines the simulations using the present model. Experimental error bars are only shown for $\phi = 1$.

The formation of hydrocarbons (see Figure 3) was only observed in the high temperature region (above 800 K). For a given temperature, their mole fractions are larger for the rich mixture and lower for the lean one. The range of products observed in the low-temperature region is more limited. These products are oxygenated species such as water, hydrogen peroxide, CO, CO₂, formaldehyde and methyl-formate (displayed in Figure 4). For most of these products, unlike hydrocarbons, mole fractions are larger under lean conditions, except for formaldehyde. For this last species, the mole fraction profile obtained under lean conditions lies between the two other profiles. Fragile species detected by Moshammer et al. [38] (e.g., hydroperoxymethyl formate, methyl-hydroperoxide and 1,3-dioxane) could not be observed in the present study due to the analytical method used here (gas chromatography).

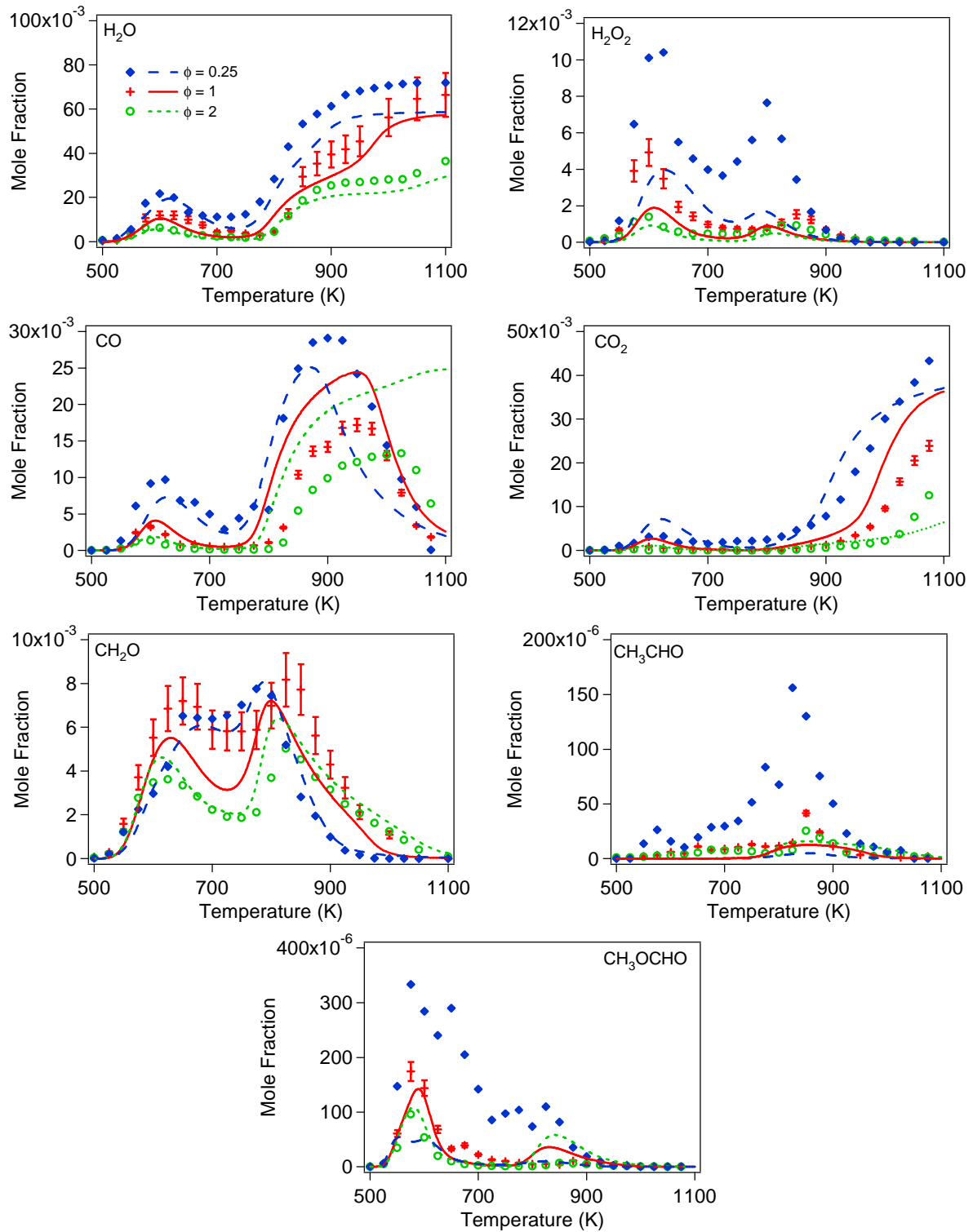


Figure 4 : Mole fractions of oxygenated reaction products ($x_{fuel} = 0.02$, $P = 106.7$ kPa, $\tau = 2$ s, $\phi = 0.25, 1$ & 2). Symbols represent experimental data and lines the simulations using the present model. Experimental error bars are only shown for $\phi = 1$.

Modeling of the oxidation of DME

Both DME oxidation models published in literature and validated for a wide range of experimental data of Table 1, were tested against experimental data obtained in this study: the first model is that of Zhao et al. [39], which was released in 2008, the second one is that of Burke et al. [22] released in 2014. Comparisons given in supplementary material show that both models over-estimate the DME reactivity in the low-temperature region whereas the agreement is good in the high-temperature region (Figure S1). A kinetic analysis of these models shows that the over predicted reactivity is mainly due to the ratio between competing reactions of the $\bullet\text{CH}_2\text{OCH}_2\text{OOH}$ radical. As far as reaction products are concerned (see Figure S1 to Figure S4), the two models well predict mole fractions of formaldehyde under rich conditions, but under-estimate them under stoichiometric and lean conditions. A similar observation can be made for hydrogen peroxide (Figure S3). Important deviations are observed for methyl-formate which is over-estimated by a factor of 10 by the model from Zhao et al. and by a factor of 3 by the model of Burke et al. [22]. The over-estimation of methyl-formate mole fractions is due to the higher reactivity predicted by both models.

A new model (90 species for 576 reactions) was developed to better account for the low-temperature oxidation chemistry of DME and is available in Supplementary Material in a pdf file (a model in CHEMKIN format can be obtained on request). This model is based on the $\text{C}_0\text{-C}_2$ reaction base which is used by software EXGAS for the automatic generation of detailed kinetic models [51]. Sub-mechanisms were added for the reactions of DME as well as reactions of primary products not already present in the $\text{C}_0\text{-C}_2$ reaction base (e.g., methyl-formate, C_3 hydrocarbons, etc...). The low-temperature oxidation reactions of DME were written following the same rules as for *n*-alkanes (starting with the addition of radical to O_2 , isomerization, and all possible subsequent reactions).

Reactions involved in the DME oxidation sub-mechanism are given in Table 3 with associated kinetic parameters. The oxidation chemistry of DME is somewhat different from that of alkanes because of the presence of the oxygen atom in the molecule which affects bond energies (Figure 5) [52–54] and which also has some effects on the kinetic parameters of reactions involving DME. As an example, the activation energy of the unimolecular initiation of DME by breaking of a C-O bond is $81.53 \text{ kcal mol}^{-1}$ at 650 K [39] which is slightly lower than the activation energy of the corresponding reaction by breaking of a C-C bond in propane ($84.46 \text{ kcal mol}^{-1}$ [55]). The activation energy of the unimolecular initiation of DME by breaking of a C-H bond is also affected by the presence of the central oxygen atom in the molecule (it is written in the reverse direction in the model).

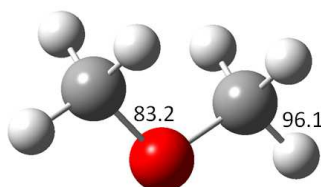


Figure 5: Bond energies in the DME molecule (kcal mol^{-1}) [52,53].

Table 3: Reactions included in the DME oxidation sub-mechanism. Kinetic parameters of the form $k = A \times T^n \times \exp(-E_a/RT)$. Units: cm^3 , mol, s, cal.

Reactions	A	n	E_a	reference
Unimolecular Initiation				
$\text{DME} = \text{CH}_3\bullet + \text{CH}_3\text{O}\bullet$	1.70×10^{42}	-7.95	91.8×10^3	[39]
$\text{CH}_3\text{OCH}_2\bullet + \text{H} = \text{DME}$	1.00×10^{14}	0	0	^a
Bimolecular Initiation				
$\text{DME} + \text{O}_2 = \text{CH}_3\text{OCH}_2\bullet + \text{HO}_2\bullet$	4.10×10^{13}	0	44.9×10^3	^b
H-atom Abstractions				
$\text{DME} + \text{H}\bullet = \text{CH}_3\text{OCH}_2\bullet + \text{H}_2$	10.96	4.00	1.8×10^3	[59]
$\text{DME} + \bullet\text{O}\bullet = \text{CH}_3\text{OCH}_2\bullet + \bullet\text{OH}$	2.69×10^7	2.00	2.6×10^3	[59]
$\text{DME} + \bullet\text{OH} = \text{CH}_3\text{OCH}_2\bullet + \text{H}_2\text{O}$	5.09×10^6	2.07	-521	[56]
$\text{DME} + \text{HO}_2\bullet = \text{CH}_3\text{OCH}_2\bullet + \text{H}_2\text{O}_2$	2.00×10^{13}	0	16.5×10^3	[39]
$\text{DME} + \text{CH}_3\bullet = \text{CH}_3\text{OCH}_2\bullet + \text{CH}_4$	26.80	3.78	9.6×10^3	[39]
$\text{DME} + \bullet\text{CHO} = \text{CH}_3\text{OCH}_2\bullet + \text{HCHO}$	2.04×10^5	2.50	13.5×10^3	^b
$\text{DME} + \text{CH}_3\text{O}\bullet = \text{CH}_3\text{OCH}_2\bullet + \text{CH}_3\text{OH}$	6.02×10^{11}	0	4.1×10^3	[8,9]
Decomposition of $\text{CH}_3\text{OCH}_2\bullet$				
$\text{CH}_3\text{OCH}_2\bullet = \text{HCHO} + \text{CH}_3\bullet$	2.22×10^{14}	-0.22	27.2×10^3	^c
Addition to O_2				
$\text{CH}_3\text{OCH}_2\bullet + \text{O}_2 = \text{CH}_3\text{OCH}_2\text{O}_2\bullet$	6.44×10^{12}	0	-91.41	[60]
Isomerization of ROO to QOOH				
$\text{CH}_3\text{OCH}_2\text{O}_2\bullet = \bullet\text{CH}_2\text{OCH}_2\text{O}_2\text{H}$	3.70	3.347	15.2×10^3	this work
$\text{CH}_3\text{OCH}_2\text{O}_2\bullet \Rightarrow \text{CH}_3\text{OCHO} + \bullet\text{OH}$	1.15×10^4	2.722	35.4×10^3	this work ^d
Decomposition of $\bullet\text{CH}_2\text{OCH}_2\text{O}_2\text{H}$				
$\bullet\text{CH}_2\text{OCH}_2\text{O}_2\text{H} \Rightarrow 2 \text{HCHO} + \bullet\text{OH}$	1.00×10^{13}	0	20.1×10^3	[61] ^e
$\bullet\text{CH}_2\text{OCH}_2\text{O}_2\text{H} = 1,3\text{-dioxetane} + \bullet\text{OH}$ ^f	4.88×10^{12}	-0.084	22.1×10^3	this work
$\bullet\text{CH}_2\text{OCH}_2\text{O}_2\text{H} = \text{CH}_3\text{OCHO} + \bullet\text{OH}$	3.55×10^{-5}	5.405	29.9×10^3	this work
Addition of $\bullet\text{CH}_2\text{OCH}_2\text{O}_2\text{H}$ to O_2				
$\bullet\text{CH}_2\text{OCH}_2\text{O}_2\text{H} + \text{O}_2 = \bullet\text{O}_2\text{CH}_2\text{OCH}_2\text{O}_2\text{H}$	7.00×10^{11}	0	0	[8,9]
Isomerization and Decomposition to Aldohydroperoxide				
$\bullet\text{O}_2\text{CH}_2\text{OCH}_2\text{O}_2\text{H} = \text{HO}_2\text{CH}_2\text{OCH}_2\text{O} + \bullet\text{OH}$	4.00×10^{10}	0	18.5×10^3	[8,9]
Termination				
$\text{CH}_3\text{OCH}_2\text{O}_2\bullet + \text{HO}_2\bullet = \text{CH}_3\text{OCH}_2\text{O}_2\text{H} + \text{O}_2$	2.00×10^{11}	0	1.3×10^3	^b
$2 \text{CH}_3\text{OCH}_2\text{O}_2\bullet = 2 \text{CH}_3\text{OCH}_2\text{O}\bullet + \text{O}_2$	1.81×10^{11}	0	-1.4×10^3	[62]
Reactions of $\text{CH}_3\text{OCH}_2\text{O}\bullet$				
$\text{CH}_3\text{OCH}_2\text{O}\bullet = \text{HCHO} + \text{CH}_3\text{O}\bullet$	9.72×10^{15}	-1.10	20.64×10^3	[8,9]
$\text{CH}_3\text{OCH}_2\text{O}\bullet = \text{CH}_3\text{OCHO} + \text{H}\bullet$	1.745×10^{16}	-0.66	11.72×10^3	[8,9]
$\text{CH}_3\text{OCH}_2\text{O}\bullet + \text{O}_2 = \text{CH}_3\text{OCHO} + \text{HO}_2\bullet$	5.00×10^{10}	0	500	[8,9]

^a rate constant taken equal to that of the recombination of H atoms with alkyl radicals as proposed by Allara and Shaw [63].

^b rate constant estimated using the rules proposed by Buda et al. [64] in the case of alkanes.

^c the A factor of this reaction proposed by [65] was divided by a factor of 2 because it was too fast.

^d the reverse reaction is not considered because the radical which would be formed is not stable and decomposes immediately to methyl-formate and $\bullet\text{OH}$ radical.

^e this reaction is actually the sum of two reactions of decomposition by β -scission with the second one being very fast. The reverse termolecular reaction is then not considered because it does not represent what happens in the reality. The A factor was lowered by a factor of 0.8.

^f this reaction is a decomposition into a cyclic ether + $\bullet\text{OH}$ radical.

H-atom abstractions by $\text{H}\bullet$, $\text{O}\bullet$, $\text{OH}\bullet$, $\text{HO}_2\bullet$, $\text{CH}_3\bullet$, $\text{CHO}\bullet$, and $\text{CH}_3\text{O}\bullet$ radicals have been considered. The literature is rich in kinetic parameters for the H-atom abstraction with $\text{OH}\bullet$ radicals, the main chain carriers. The rate constant used in this model has been taken from Olzmann et al. [56], whereas Zhao et al. used the older value from Tranter and Walker [57]. This rate constant was also tested in our model and no difference was observed in the predicted reactivity and product selectivity. The rate constant for the H-atom abstraction involving a methyl radical is that used by Zhao et al. in their model. A test with the rate parameters proposed by Tranter et al. [58] (the difference is the A factor which is lowered by a factor of 2.6) was attempted. This change resulted in a slightly lower reactivity (mostly visible above 800 K in flow reactor simulations) and in longer ignition delay times around 1000 K).

Due to its structure, the $\text{CH}_3\text{OCH}_2\bullet$ radical obtained by H-atom abstraction can undergo only a few types of reactions: decomposition by β -scission forming formaldehyde and the methyl radical, or addition to O_2 forming a peroxy radical ($\text{CH}_3\text{OCH}_2\text{O}_2\bullet$ in Table 3). The reaction with O_2 yielding $\text{HO}_2\bullet$ radical and an alkene is not possible for DME as there is no abstractable H-atom on the central oxygen atom. The absence of this reaction type has important repercussions on the fuel reactivity in the low-temperature region.

The two possible reactions of intramolecular isomerization of the $\text{CH}_3\text{OCH}_2\text{O}_2\bullet$ radical have been written in the model although one of them is not favored since it involves shifting an H-atom from the $-\text{CH}_2-$ group. This isomerization leads to a radical which is not stable and which decomposes right away to methyl-formate (CH_3OCHO in Table 3) and $\text{OH}\bullet$ radical. The other isomerization which shifts an H-atom of the terminal $-\text{CH}_3$ group forms an hydroperoxy radical ($\bullet\text{CH}_2\text{OCH}_2\text{O}_2\text{H}$ in Table 3) which can lead after several steps (second addition to O_2 , isomerization and decomposition) to the formation of an aldohydroperoxide ($\text{HO}_2\text{CH}_2\text{OCH}_2\text{O}$ in Table 3) which is a branching agent. As far as decomposition reactions of the $\bullet\text{CH}_2\text{OCH}_2\text{O}_2\text{H}$ radical are concerned, the β -scission decomposition to $2 \text{CH}_2\text{O} + \text{OH}\bullet$ was considered as in previous works (e.g. [9,39]) and a reaction of decomposition to a cyclic ether (1,3-dioxetane) and $\text{OH}\bullet$ was added.

Theoretical calculations were performed to obtain a new reliable set of kinetic parameters for four reactions (see Table 3) as well as thermodynamic data of species involved in these reactions. Calculations were carried out from the G4 method [66] implemented in the software Gaussian 09 [67]. Intrinsic reaction coordinates calculations were performed to ensure that the transition states correctly connect reactants and products. For each reaction, the lower energy conformers (reactants and transition states) have been sought by means of relaxed scans around single bonds. Transmission coefficients for reactions involving an H-transfer have been computed from the 1D-Eckart method [68] and low frequencies, corresponding to internal rotations, have been treated by means of the Pitzer and Gwinn approximation [69] for hindered rotors. Finally, kinetic parameters were obtained, from the software CHEMRATE [70], by fitting the rate constant values obtained from the canonical transition state theory at several temperatures using the modified-Arrhenius model.

Reactions theoretically investigated were the $\text{RO}_2\bullet$ to $\bullet\text{QOOH}$ radical isomerizations, as well as the $\bullet\text{QOOH}$ radical decompositions to give 1,3-dioxetane or methyl-formate, for which there were very few data in literature. Figure 6 displays a schematic potential energy surface of the $\text{CH}_3\text{OCH}_2\bullet + \text{O}_2$ system with reactions taken into account in the present model. It is obvious that the isomerization reaction through the transition state TS2 ($\text{CH}_3\text{OCH}_2\text{OO}\bullet$ to $\text{CH}_3\text{OCHO} + \text{OH}\bullet$) is rather difficult and that

the isomerization through TS1 ($\text{CH}_3\text{OCH}_2\text{OO}\bullet$ to $\text{CH}_2\bullet\text{OCH}_2\text{OOH}$) is the easiest consumption route for the $\text{CH}_3\text{OCH}_2\text{OO}\bullet$ radical. As far as unimolecular consumption reactions of the $\text{CH}_2\bullet\text{OCH}_2\text{OOH}$ radical are concerned, the isomerization through TS3 has a very high barrier compared to the two other decomposition channels (to 1,3-dioxetane + $\bullet\text{OH}$ and formaldehyde + $\bullet\text{OH}$). Eskola et al. [71], who investigated the $\text{CH}_3\text{OCH}_2\bullet + \text{O}_2$ system, proposed a similar potential energy surface. They did not take into account the two difficult isomerizations (through TS2 and TS3), but they found two decomposition routes to $2 \text{CH}_2\text{O} + \bullet\text{OH}$. The two difficult isomerizations have been considered in the present models although they are certainly less important.

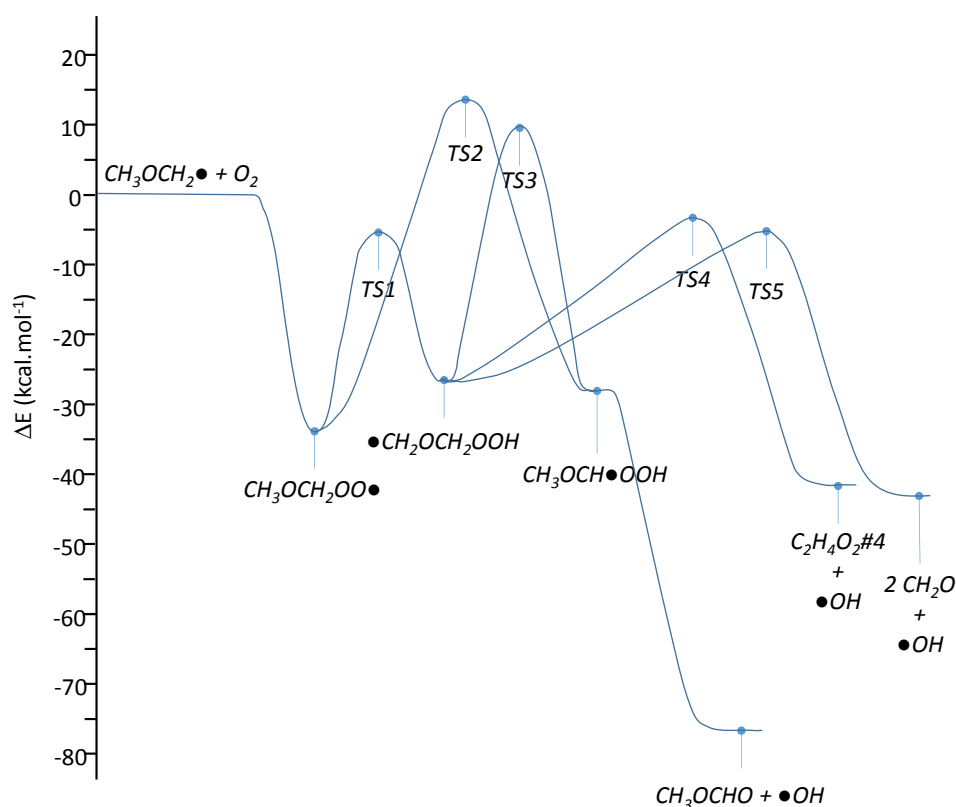


Figure 6: Schematic potential energy surface of the $\text{CH}_3\text{OCH}_2\bullet + \text{O}_2$ system. Reactions through TS1, TS2 and TS3 are isomerizations, that through TS4 is a decomposition to 1,3-dioxetane ($\text{C}_2\text{H}_4\text{O}_2\#4$) + $\bullet\text{OH}$ and that through TS5 is a β -scission.

Reactions in the methyl-formate sub-mechanism are given in Table S1. As for dimethylether, initiation reactions and H-atom abstraction were considered. Two radicals can be obtained from methyl-formate: $\text{CH}_3\text{OC}\bullet\text{O}$ and $\bullet\text{CH}_2\text{OCHO}$ radicals. The $\text{C}_0\text{-C}_2$ reaction base already contained decomposition reactions of the $\text{CH}_3\text{OC}\bullet\text{O}$ radical. Reactions of addition to O_2 have been added as well as reactions of the other radical ($\bullet\text{CH}_2\text{OCHO}$) which was not present in the $\text{C}_0\text{-C}_2$ reaction base. Reactions have also been added for the consumption of 1,3-dioxetane. These reactions are H-atom abstractions (by $\bullet\text{OH}$, $\text{H}\bullet$, $\bullet\text{O}\bullet$ and $\text{HO}_2\bullet$ radicals) and the molecular decomposition to give formaldehyde. The rate constant of the molecular reaction was theoretically calculated in the present work: $k = 3.92 \times 10^{12} \times T^{0.676} \times \exp(-39834/RT)$ in cm^3 , mol, s, cal units. Rate constants of H-atom abstractions were estimated from those of dimethylether taking into account that both species are ethers, whether they are cyclic or not. No calculation was carried out for H-atom abstraction because this 1,3-dioxetane was

only detected in small amounts. The reactions for the formation and consumption of formaldehyde, which is one of the main reaction products, were already present in the C₀-C₂ reaction base. Kinetic parameters of the reaction of H-atom abstraction from CH₂O by HO₂• radicals are those recommended by Baulch et al. [55] with the A-factor divided by a factor of 2. This modification was necessary to have a better prediction of the reactivity in the high temperature region (the change has no effect at low-temperature).

Discussion

The model described in the previous part of the paper is available on request. Simulations using this model were performed with the different calculation modules in Chemkin II [72]. Predictions were compared with new jet-stirred reactor data obtained in this study, as well as a wide range of existing data from the literature. The model developed in this study was used to perform a kinetic analysis and to better understand the oxidation chemistry of DME.

Comparison with jet-stirred reactor data obtained in the present study

Model predictions for jet-stirred reactor data obtained in this study are displayed in Figure 2 to Figure 4. It can be seen that the model well reproduces the global reactivity, as well as the influence of equivalence ratio (Figure 2). As far as the formation of hydrocarbons is concerned (Figure 3), the agreement is overall satisfactory in the lean and stoichiometric mixtures whereas deviations are observed for the rich mixture. For the rich mixture mole fractions of C₀-C₂ species are over-estimated (a factor of about 2 for CH₄, C₂H₄ and C₂H₆) whereas those of C₃ species (propane and propene) are under-estimated by a factor of about 2. In contrast to model predictions, the formation of propene was not observed under lean conditions due to experimental mole fractions below the detection limit. The agreement is overall satisfactory for oxygenated products (Figure 4). Mole fractions of water are well reproduced in the low temperature region (below 850 K), but are under-estimated above this temperature, especially under lean conditions (there is a factor of about 1.3). These discrepancies can be explained by the experimental uncertainties which are significantly larger in this temperature zone. Deviations can be spotted for hydrogen peroxide and acetaldehyde which are under-estimated by the model whatever the equivalence ratio, but the leaner the mixture, the larger the deviation. As an example, under lean conditions (worst case), the spotted deviations are a factor of 2.5 for H₂O₂ and a factor of 50 for acetaldehyde. Note that this last species is formed in very low amounts and that the mole fractions of trace products are more sensitive to model parameter uncertainties. Formaldehyde mole fractions are well reproduced for the lean and rich conditions, but slightly under-estimated at $\varphi = 1$ in the negative coefficient temperature zone (less than a factor of 2). There is no obvious explanation for these discrepancies at $\varphi = 1$. The correct agreement obtained at the two other φ gives confidence in data recorder at $\varphi = 1$. A possible reason could be specificities missed in the complex low-temperature oxidation chemistry of DME. CO mole fractions are over-predicted at $\varphi = 1$ and 2, and under-predicted under the lean conditions. This could be due to reactions of formaldehyde which have not be revisited in this work. Mole fractions of methyl-formate, which is a minor product as acetaldehyde, are well reproduced for the rich and stoichiometric conditions, but under-estimated at $\varphi = 0.25$ by a factor of about 5.

Simulation uncertainty and sensitivity analyses

The global sampling approach based on low discrepancy sequences which has been proposed by Hébrard et al. [74] has been applied in order to propose error bars on JSR simulations. A two parameter uncertainty factor has been assigned to each considered rate constant. An uncertainty factor $F(T)$ of a reaction rate constant $k(T)$ was estimated at any given temperature following an expression adapted from [75]:

$$F(T) = F(300K) \exp \left| g \left(\frac{1}{T} - \frac{1}{300} \right) \right| \quad (1)$$

where $F(300K)$ is the uncertainty in the rate constant $k(T)$ at $T = 300$ K and g is the "uncertainty-

extrapolating" coefficient used to obtain the rate constant uncertainty $F(T)$ at different temperatures. The uncertainty factors for reactions of the C₀-C₂ reaction base were directly taken from [74] and were mainly provided by the evaluation made by Baulch et al. [76]. In line with the approach considered by [74], for the kinetic parameters used within the DME sub-mechanisms, factors $F = 1.26$, $g = 0$ were considered for unimolecular or bimolecular initiations and additions with oxygen, whereas $F = 1.12$, $g = 100$ were taken into account otherwise. Thousands simulations were then run for 25 studied temperatures between 500 and 1100 K, quasi-randomly varying the 576 rate constants in the limits of their given uncertainties.

Figure 7 presents the JSR mole fractions predicted using the quasi-random sample proposed by [74] for some representative species (fuel, H₂O, H₂O₂, CO, CO₂, CH₂O and methyl formate). The predicted errors bars below 780 K are small (less than $\pm 5\%$) for all the studied species, except for formaldehyde and methyl formate for which they are significantly larger (up to about ± 10 and $\pm 15\%$, respectively). Note that the uncertainties used in DME sub-mechanisms are likely optimistic and that using some larger uncertainty values for some sensitive rate constants could influence these predicted error bars.

The predicted error bars on fuel consumption and product formation become larger above 780 K, especially for H₂O, formaldehyde, CO and CO₂ production. This is likely due to the fact that, in this intermediate temperature range, a maximum number of reactions are playing a role in the production of the radical pool and the formation of light species. Note that none of the reactions involved in water, formaldehyde and CO production have a notably larger uncertainty. The large predicted error bars which can be spotted for CO₂ are directly related to those seen for CO. Surprisingly, the predicted error bars on H₂O₂ and methyl formate are less affected by temperature than those of other species, indicating probably that a more limited number of reactions are involved in their formation and consumption.

As proposed by [74], a global screening approach based on Spearman Rank Correlation Coefficients was also performed. RCCs [77] provide a measure of the strength of the non-linear relationship between model inputs and target outputs, by assessing how well the relationship between two variables can be described using a monotonic function. The RCC threshold was set to 0.2 to give a reasonable yet restricted set of significant reactions as shown in Table S2 for simulated JSR DME mole fractions. 35 reactions were then identified, 21 from the C₀-C₂ reaction base and 14 from the DME sub-mechanisms, including 4 H-abstractions from DME, as well as 5 reactions involving CH₃OCH₂O₂• or •CH₂OCH₂O₂H radicals. Tomlin et al., who performed an evaluation of the combustion chemistry of DME using global uncertainty and sensitivity analyses [73], also observed that the low-temperature oxidation chemistry of DME is complex as all reactions involved in this chemistry contribute in uncertainties in predicted mole fractions.

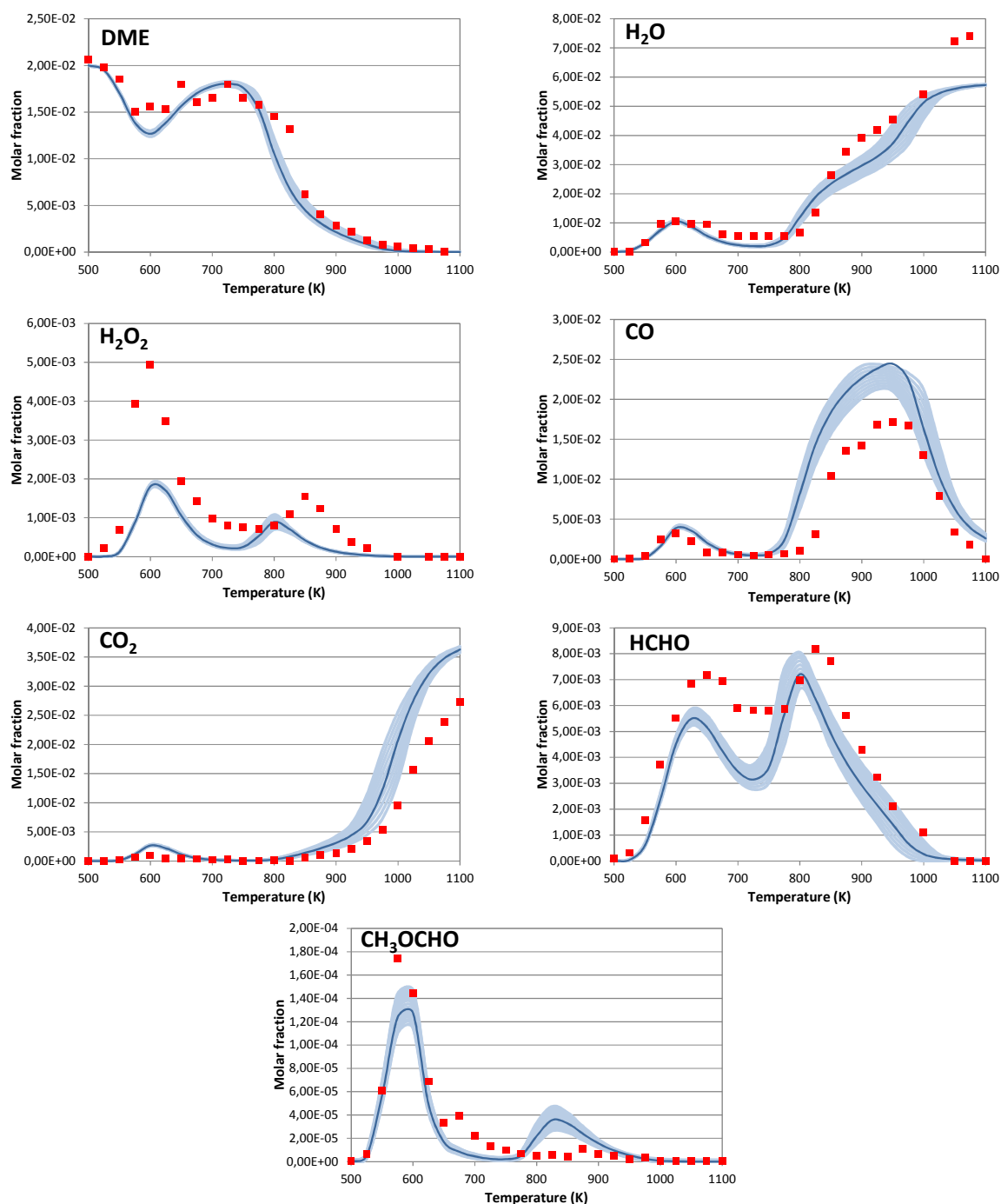


Figure 7: Error bars on the predicted mole fraction profiles vs. temperature of some representative products under the conditions of figures 2 to 4. Blue solid lines: nominal and mean profiles. Shaded area corresponds to the standard deviation (1σ) of the modeled results. Symbols represent experimental data and lines the simulations using the present model.

Kinetic analysis of the model

A kinetic analysis of the DME mechanism was performed in order to better understand the chemistry which is involved in the oxidation of this species as well as the probable reasons for the discrepancies observed when comparing computed and experimental data. Reaction path diagrams were drawn at low (625 K) and high (850 K) temperatures (Figure 8) and also for the three studied equivalence ratios

(Figure S5 in Supplementary Material). In all cases the fuel is mainly consumed by H-atom abstraction reactions forming the $\text{CH}_3\text{OCH}_2\bullet$ radical. This radical reacts in different ways according to the conditions:

- At low temperature (650K), the $\text{CH}_3\text{OCH}_2\bullet$ radical mainly adds to O_2 to form the $\text{CH}_3\text{OCH}_2\text{OO}\bullet$ radical which isomerizes to $\bullet\text{CH}_2\text{OCH}_2\text{OOH}$. This radical reacts either by decomposition (C-O β -scission forming formaldehyde or decomposition to 1,3-dioxetane) or by a second addition to O_2 forming a $\bullet\text{OOCH}_2\text{OCH}_2\text{OOH}$. Note that the ratio between decomposition and the second addition to O_2 is crucial for well accounting the global reactivity. $\bullet\text{OOCH}_2\text{OCH}_2\text{OOH}$ radical reacts by isomerization and decomposition to yield $\bullet\text{OH}$ radical and the aldehydohydroperoxide (HOCH_2OCHO) detected by Moshhammer [38]. The decomposition of the aldehydohydroperoxide leads to the formation of formaldehyde and CO_2 .
- At high temperature (800K), the low-temperature chemistry still plays a role but the main reaction consuming $\text{CH}_3\text{OCH}_2\bullet$ radical is the decomposition by C-O β -scission forming formaldehyde and $\bullet\text{CH}_3$ (this is 85.6 % of the consumption of the $\text{CH}_3\text{OCH}_2\bullet$ radical at 850 K with importance increasing with temperature).

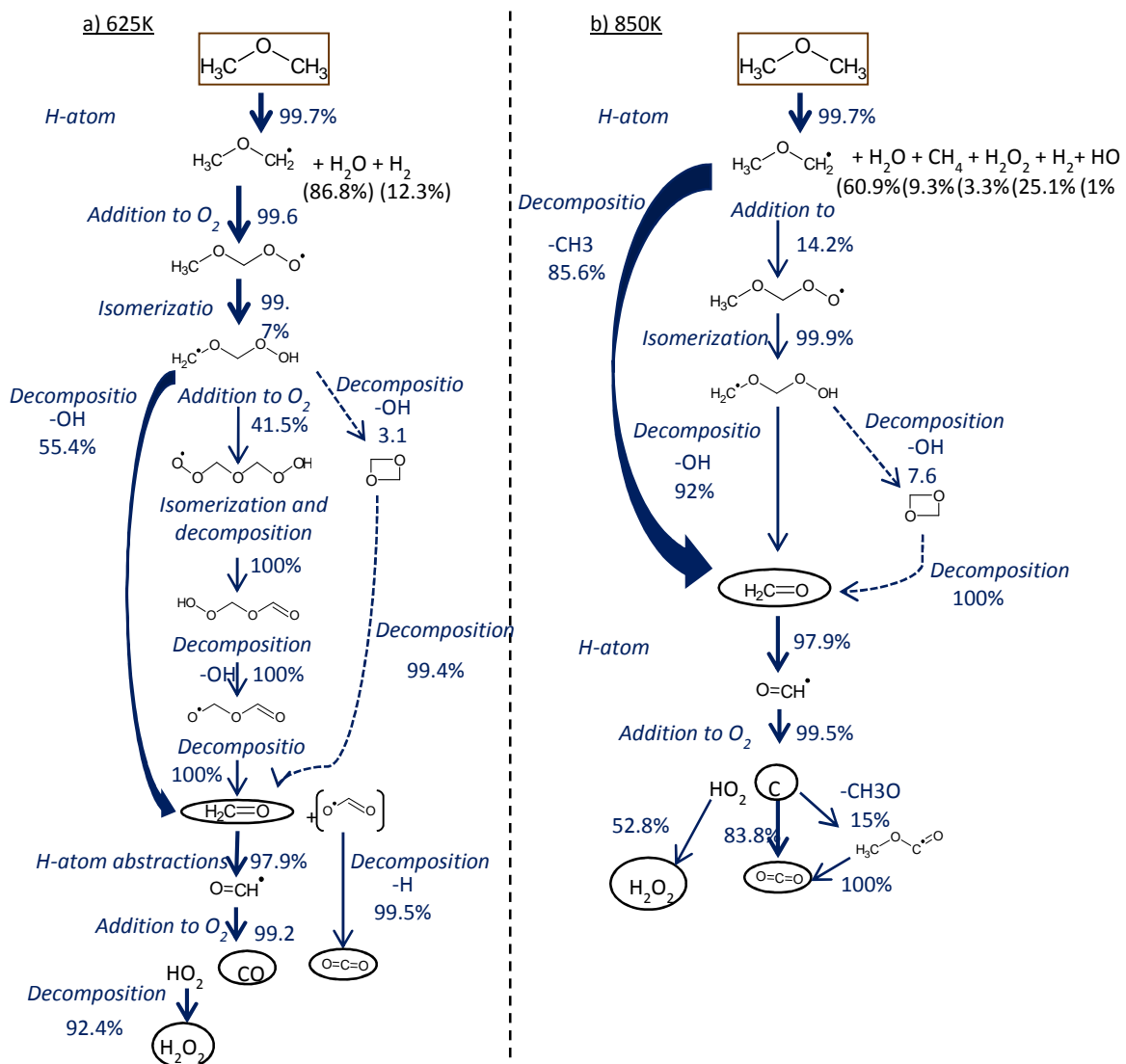


Figure 8: Comparison of data flux analysis at (a) low- and (b) high-temperature ($\varphi = 1$).

The ways of formation of formaldehyde, one of the main intermediates in DME oxidation, also depend on the temperature range. At low temperature (e.g., 625 K), it is mainly formed from the decomposition of the $\bullet\text{CH}_2\text{OCH}_2\text{OOH}$ to yield two formaldehyde molecules and $\bullet\text{OH}$ (79%). It is also formed from the decomposition of the $\bullet\text{OCH}_2\text{OCHO}$ radical to give formaldehyde and $\bullet\text{OCHO}$ (16%). The $\bullet\text{OCH}_2\text{OCHO}$ radical is obtained from the decomposition of the aldohydroperoxide ($\text{HOOCH}_2\text{OCHO}$) formed in the low temperature oxidation of DME. At high temperature (e.g., 825 K), formaldehyde is mainly formed from the decomposition of the $\text{CH}_3\text{OCH}_2\bullet$ radical (45%). The decomposition of the $\bullet\text{CH}_2\text{OCH}_2\text{OOH}$ radical is still responsible for 27% of the production of formaldehyde. A third production route (25%) is the decomposition of the $\text{CH}_3\text{O}\bullet$ radical (obtained from the reaction of $\text{CH}_3\bullet$ and $\text{HO}_2\bullet$ radicals). Note that discrepancies between experimental and computed mole fractions are only visible at $\varphi = 1$ below 800 K. Otherwise the model gives a good prediction of experimental mole fractions. There is no obvious reason that could explain these deviations at $\varphi = 1$.

The relatively high mole fractions of H_2O_2 observed during experiments can seem surprising. Indeed, during alkane oxidation, this species is mainly formed from $\text{HO}_2\bullet$ radicals which comes from reactions " $\text{R}\bullet + \text{O}_2 \rightleftharpoons \text{olefin} + \text{HO}_2\bullet$ " which are not present in the case of DME due to the structure of the fuel as already stated in the paper. The kinetic analysis of the model ($\varphi = 1$) showed that $\text{HO}_2\bullet$ radicals are mainly produced by the reactions of $\bullet\text{CHO}$ radicals with O_2 yielding $\text{CO} + \text{HO}_2\bullet$ (this channel represents 79.2% of the formation of this radical at 625 K and 90.0% at 850 K). Kinetic parameters of this reaction are those proposed by Timonen et al. [78]. A test with the kinetic parameters proposed by Tsang et al. [79] has resulted in no change in the reactivity and product distribution. $\bullet\text{CHO}$ radicals are particularly abundant given that they are formed by H-atom abstractions from formaldehyde which is one of the main products from the oxidation of DME. Note that the most sensitive reaction for the formation of H_2O_2 in the high temperature region is the H-atom abstraction from CH_2O by $\text{HO}_2\bullet$ yielding $\bullet\text{CHO}$ and H_2O_2 . Most sensitive reactions in the low-temperature region are reactions promoting the global reactivity of the system like H-atom abstractions of the fuels and reactions involved in the branching chain (addition to O_2 , decomposition of the aldohydroperoxide).

Figure 9 displayed the main pathways for the formation of methyl-formate at low-temperature (JSR, 625 K, $\varphi = 1$). Methyl-formate is formed through three main pathways. The most important is the recombination of $\text{CH}_3\text{O}\bullet$ and $\bullet\text{CHO}$ radicals (43.0%). The second formation channel is the decomposition (by C-H β -scission) of the $\text{CH}_3\text{OCH}_2\text{O}\bullet$ radical which comes from disproportionation reactions of two $\text{CH}_3\text{OCH}_2\text{OO}\bullet$ radicals and of $\text{CH}_3\text{OCH}_2\text{OO}\bullet$ and $\text{HO}_2\bullet$ radicals (36.5%). Note that these $\text{CH}_3\text{OCH}_2\text{OO}\bullet$ consumption channels are not visible in the diagram in Figure 8 because they represent only very small consumption routes compared to the $\text{RO}_2\bullet$ to $\bullet\text{QOOH}$ isomerization. The last channel is the combination of the $\bullet\text{OCHO}$ and $\bullet\text{CH}_3$ radicals. The $\bullet\text{OCHO}$ radical mainly comes from the decomposition of the $\bullet\text{OCH}_2\text{OCHO}$ radical obtained from the decomposition of the aldohydroperoxide which is formed in the low-temperature oxidation of DME (20.2%). According to the rate of production analysis, the direct formation of methyl-formate through the isomerization of the $\text{CH}_3\text{OCH}_2\text{OO}\bullet$ radical does not play a role. This was expected given the very high energy barrier of the reaction. As stated previously, the model under-predicts the mole fractions of methyl formate under lean conditions. According to the kinetic analysis performed at 625 K, the formation and consumption fluxes are very similar under stoichiometric and lean conditions, with no clear evidence of what could explain the under-estimation at $\varphi = 0.25$. The $\text{CH}_3\text{OCH}_2\text{O}\bullet + \text{O}_2$ to methyl formate + $\text{HO}_2\bullet$ reaction is included in

the model but does not play a role. Kinetic parameters used for this reaction are from the work of Zhao et al. [39]. Uncertainties in these kinetic parameters could possibly explain the under-estimation of methyl formate. Another intermediate observed in small amounts and significantly under-estimated by the model is acetaldehyde (Figure 4). According to the kinetic analysis at 850 K ($\varphi = 1$), acetaldehyde is mainly formed from the $\text{CH}_3\text{CH}_2\text{O}\cdot$ radical (through C-H β -scission, 69%). The $\text{CH}_3\text{CH}_2\text{O}\cdot$ radical is obtained from the addition of the methyl radical to formaldehyde. The kinetic parameters for this reaction are those proposed by Baulch et al. [80]. Revisiting reactions of formaldehyde would be probably beneficial for a better prediction of acetaldehyde. Secondary pathways to acetaldehyde are the reaction of the ethyl radical and O_2 (8%), the disproportionation of $\text{HO}_2\cdot$ and $\cdot\text{CH}_2\text{CHO}$ radicals (8%) and the reaction of C_2H_4 and $\text{HO}_2\cdot$ radical (8%). Note that the large underprediction of acetaldehyde can also indicate a missing formation pathway in the model.

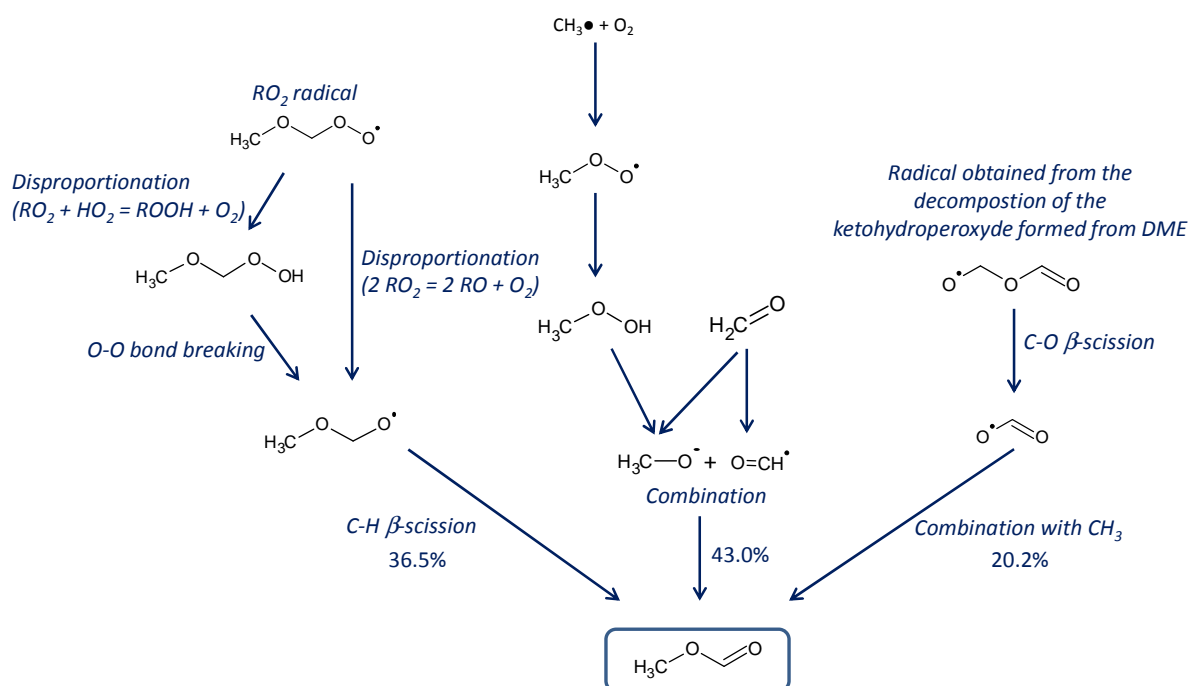


Figure 9: Main pathways for the formation of methyl-formate (JSR, $\varphi = 1$ and temperature of 625K).

Figure S5 displays reaction path diagrams for the oxidation of DME at 625 K for the three studied equivalence ratios (0.25, 1 and 2). Overall, these diagrams show that the equivalence ratio also has an important impact on the DME oxidation. The increase of the inlet oxygen mole fraction (with constant fuel inlet mole fraction) has a limited effect on the relative consumption of the $\text{CH}_3\text{OCH}_2\cdot$ radical through the first addition to O_2 (it is 99.1% at $\varphi = 2$, 99.6% at $\varphi = 1$ and 99.9% at $\varphi = 0.25$). This limited effect is due to the impossibility of the $\text{CH}_3\text{OCH}_2\cdot$ radical to react through oxidation reactions ($\text{R}\cdot + \text{O}_2 = \text{olefin} + \text{HO}_2\cdot$) which are inhibiting channels in competition with the first addition to O_2 , as it can be observed during the oxidation of fuels such as alkanes. The equivalence ratio has an important effect on the relative consumption of the $\cdot\text{CH}_2\text{OCH}_2\text{OOH}$ radical. The second addition is favored under lean conditions in detriment to decomposition (the addition to O_2 accounts for 26.2% of the consumption of the $\cdot\text{CH}_2\text{OCH}_2\text{OOH}$ radical at $\varphi = 2$, 41.5% at $\varphi = 1$ and for 75.5% at $\varphi = 0.25$). This favored addition to O_2 is responsible for the enhanced reactivity under lean conditions.

Comparison with data from literature

Model predictions were compared against several sets of data published in literature covering a large range of conditions. Overall the performance of the present model is as satisfactory as those of previous literature models for high temperature data given that the high temperature chemistry used is very similar. The low-temperature chemistry used in the present model enables a better prediction of the reactivity in this specific region as it solves the over-estimation observed when using literature models.

- Jet-stirred reactor comparison

A comparison was made using jet-stirred reactor oxidation data from Dagaut et al. [37] at 10 bars, over the temperature range 500 – 800 K (Figure 10). The agreement is quite good in the region before the negative temperature coefficient (from 500 to 600 K) for the fuel, whereas mole fraction of CO, CO₂ and CH₂O are under-predicted. Above 600 K, the model over-predicts the reactivity. Note that experimental fuel mole fractions might have a large uncertainty since some of them are larger than 0.002 (fuel inlet mole fraction) in the temperature range 700 – 800 K, which is not possible.

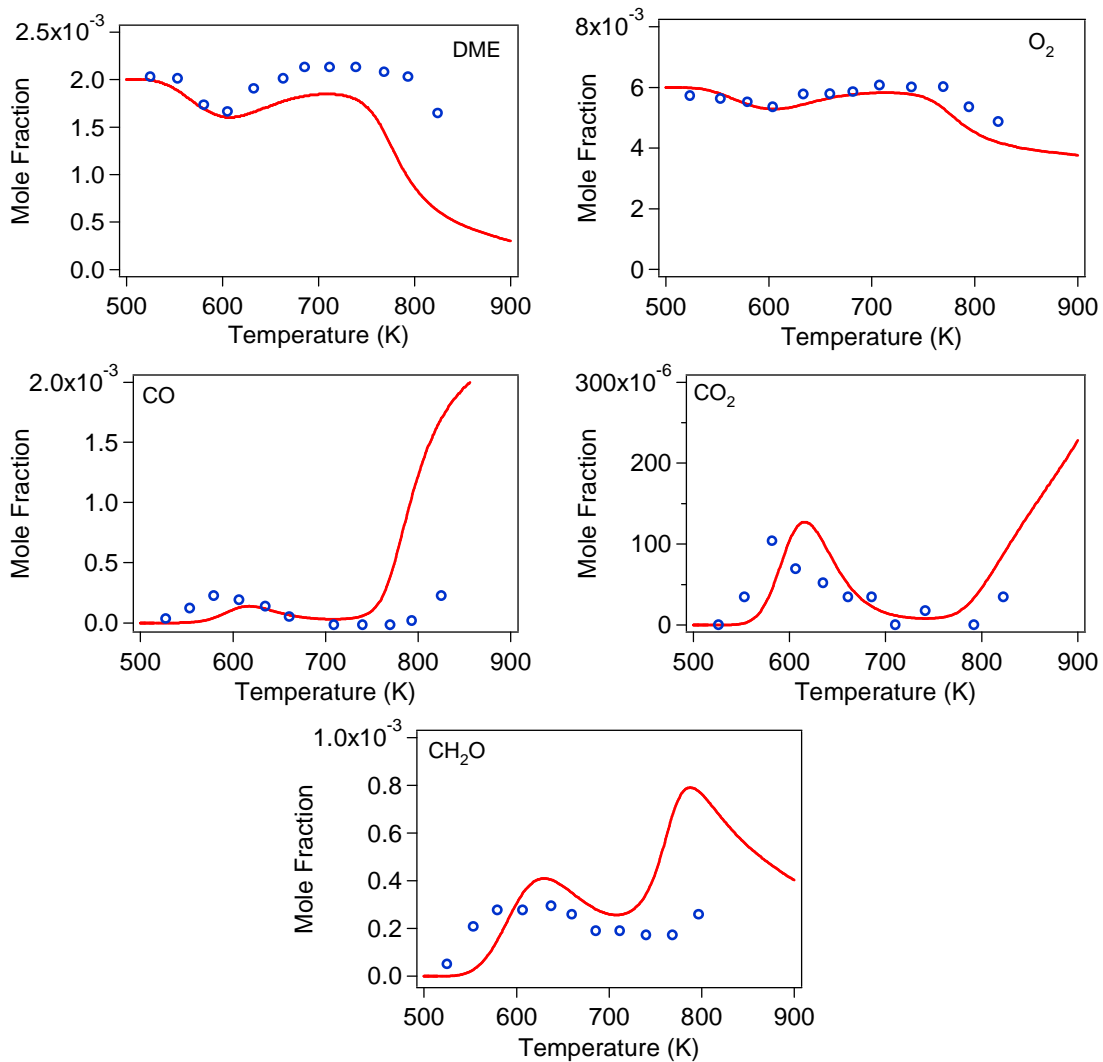


Figure 10: Comparison with jet-stirred reactor data from Dagaut et al. [37] ($P = 10$ bars, $\tau = 1$ s, $\varphi = 1$, 2000 ppm DME, 6000 ppm O₂, dilution in N₂). Symbols represent literature experimental data and lines the simulations using the present model.

In the same way the conversion of the fuel occurs between 550 and 575 K, whereas the production of CO, CO₂ and CH₂O occurs before 550 K, which is not consistent. Note that the formation of formaldehyde was observed in the negative temperature coefficient region whereas the fuel mole fraction profile shows no reactivity. This confirms that uncertainties in fuel mole fractions were rather important.

- Flow reactor comparisons

Figure 11 displays the comparison with flow reactor oxidation data from Alzueta et al. [7] at atmospheric pressure, in the high temperature region (800 to 1300 K). It can be seen that the model well reproduces the reactivity of the fuel as well as the formation of CO and CO₂. The good agreement with these data is not surprising as the major changes in the model developed in this study compared to previous ones, especially Zhao et al. [9], mainly concerns low-temperature oxidation chemistry.

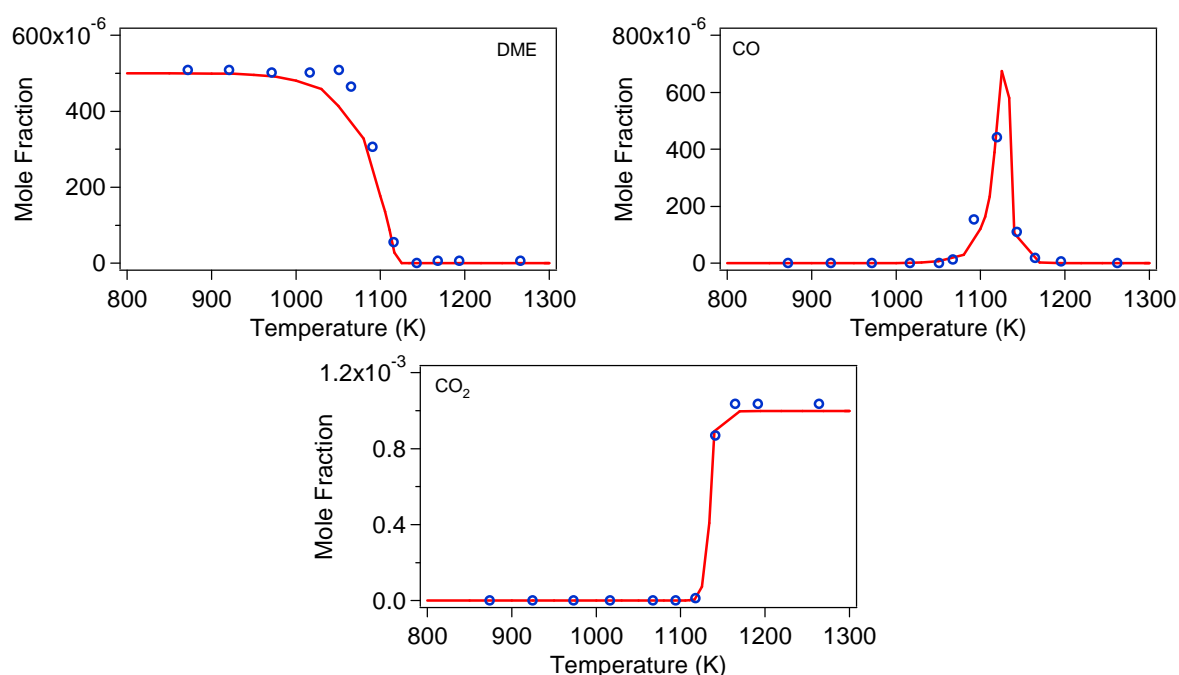


Figure 11: Comparison with flow reactor data from Alzueta et al. [7] ($P = 1 \text{ atm}$, $\tau = 188 \text{ ms}$, 500 ppm DME, 3000 ppm O₂, 3.34% water, dilution in N₂). Symbols represent literature experimental data and lines the simulations using the present model.

The comparison with flow reactor oxidation data from Curran et al. [9] at a pressure of 12.5 atm and at temperatures from 500 to 800 K is shown in Figure 12. The low-temperature chemistry of dimethylether was investigated in this study. The comparison shows that a satisfactory agreement is obtained. The reactivity is slightly over-estimated in the negative temperature coefficient region (between 600 and 675 K). Water, CO and CH₄ mole fractions are rather well reproduced whereas CO₂ and formaldehyde mole fractions are over-estimated by factors of about 10 and 5, respectively, at 625 K. According to the kinetic analysis performed at 625 K and a residence time of 2 s, these two species are simultaneously produced from the $\bullet\text{OCH}_2\text{OCHO}$ radical which is obtained from the decomposition of the HOCH_2OCHO aldehydoperoxide obtained in the low-temperature oxidation of DME. Note that the most sensitive reaction by far in the formation of CO₂ under these conditions is the second addition of the $\bullet\text{CH}_2\text{OCH}_2\text{OOH}$ radical to O₂ yielding the $\bullet\text{OOCH}_2\text{OCH}_2\text{OOH}$ radical which is the precursor of the HOCH_2OCHO aldehydoperoxide.

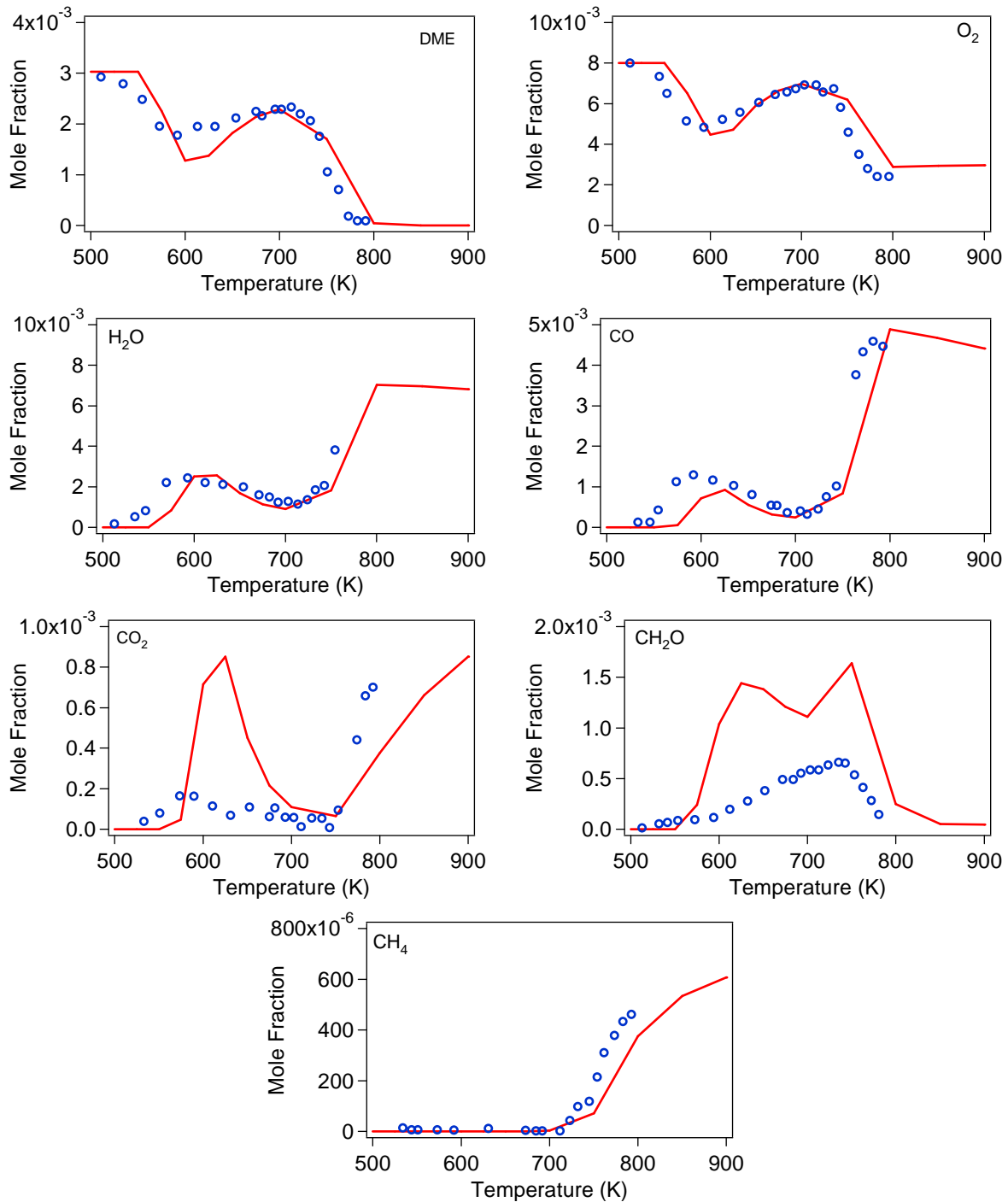


Figure 12: Comparison with flow reactor data from Curran et al. [9] ($P = 12.5$ atm, $\tau = 1.8$ s, $\varphi = 1.13$, 3030 ppm DME, 8000 ppm O₂, dilution in N₂). Symbols represent literature experimental data and lines the simulations using the present model.

Figure 13 displays comparison against flow reactor oxidation data obtained by Herrmann et al. [12] at quasi atmospheric pressure over the temperature range 400 - 1200 K. The reactivity of the system is under-estimated in the zone following the negative temperature coefficient region (750 – 900 K): the model predicts that the reactivity returns to zero whereas experiments show some reactivity in this region. Reaction product mole fractions are rather well reproduced by the model.

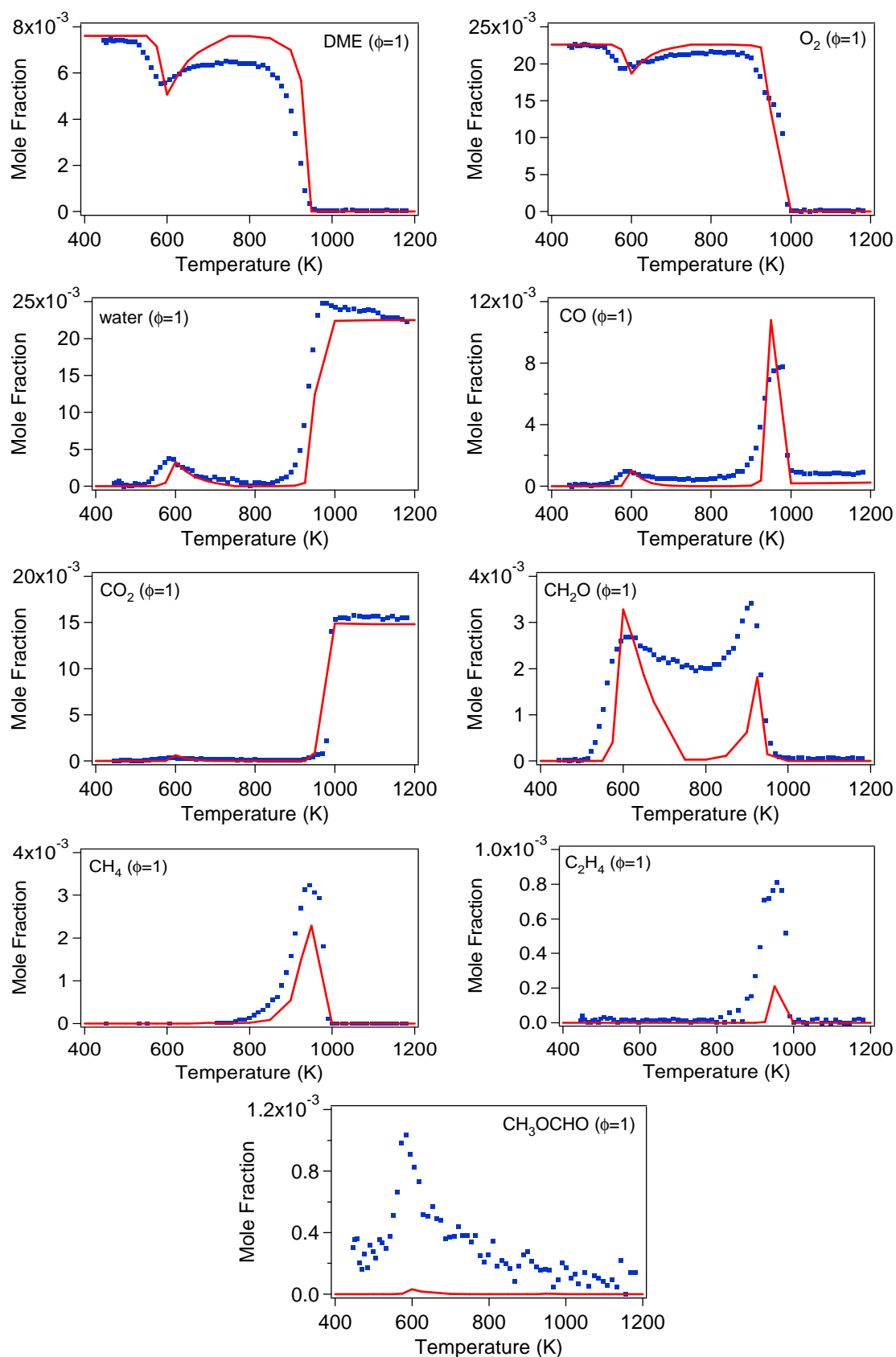


Figure 13: Comparison with flow reactor data from Herrmann et al. [12] ($P = 0.97$ bars, $\tau = 0.9 - 2.9$ s, $\phi = 1$, 7613 ppm DME, 22590 ppm O₂, dilution in Ar). Symbols represent literature experimental data and lines the simulations using the present model.

Some deviations are observed for formaldehyde, in particular in the negative temperature coefficient region. Only ethylene and methyl-formate mole fractions are significantly under-estimated by the model. Note that the methyl-formate mole fractions obtained by Herrmann et al. were very important (same order of magnitude as formaldehyde) whereas the formation of methyl-formate in the present JSR study was 30 times lower than that of formaldehyde. There is no obvious explanation for these different behaviors.

Data computed using the model were compared with recent flow reactor data from Kurimoto et al. [16] with H₂O₂ quantification (Figure 14). Simulations were performed using actual residence times provided by the authors. Except the temperature shift which is observed at low-temperature, the agreement is overall satisfactory for the two studied equivalence ratio ($\varphi = 0.2$ and 1.06). The model predicts correct maximum mole fractions for H₂O₂ at low-temperature at $\varphi = 1.06$ (but it is over-estimated at $\varphi = 0.2$). Computed and experimental mole fractions for HO₂• (only quantified at low-temperature and at $\varphi = 0.2$) are of the same order of magnitude. Methyl-formate mole fractions are under-estimated by a factor of about 4. Note that mole fractions of methyl formate are not of the same order of magnitude as formaldehyde, contrary to what was observed by Herrmann et al. [12]. There is a factor of about 20 between the maximum mole fractions of these two species at low-temperature under stoichiometric conditions which is of the same magnitude order than the factor of ≈ 40 obtained with present JSR data.

Comparison with pyrolysis data from Fischer et al. [8] are shown in Figure S6 in supplementary material. A good agreement is obtained for the fuel decomposition if a shift of 50 ms is used as recommended by the authors. Deviations are observed in the selectivity of the reaction products. As an example the formation of species, such as CO, CH₂O and CH₄, is over-estimated by the model whereas that of CO₂, ethylene and ethane is under-estimated.

- Shock tube and rapid compression machine comparisons

Comparisons with shock tube data from Pfahl et al. [18] at 13 and 40 bars are displayed in Figure 15. The temperature range investigated in this study covers both the low and high-temperature regions. Ignition delay times calculated using the model presents a good agreement with these data at both pressures. Computed ignition delay times are slightly over-estimated at low-temperature, but the model well reproduces the negative temperature coefficient behavior. This assesses the performance of the model for the prediction of the global reactivity.

Figure 16 shows the comparison with shock tube data from Li et al. [19] at 22 bars and at several equivalence ratios. These data are complementary to that of Pfahl et al. [18] as they were obtained under similar conditions, except pressure. Again the agreement is overall satisfactory whatever the temperature and the model well reproduces the negative temperature coefficient behavior with a slight over-estimation observed in stoichiometric and rich conditions.

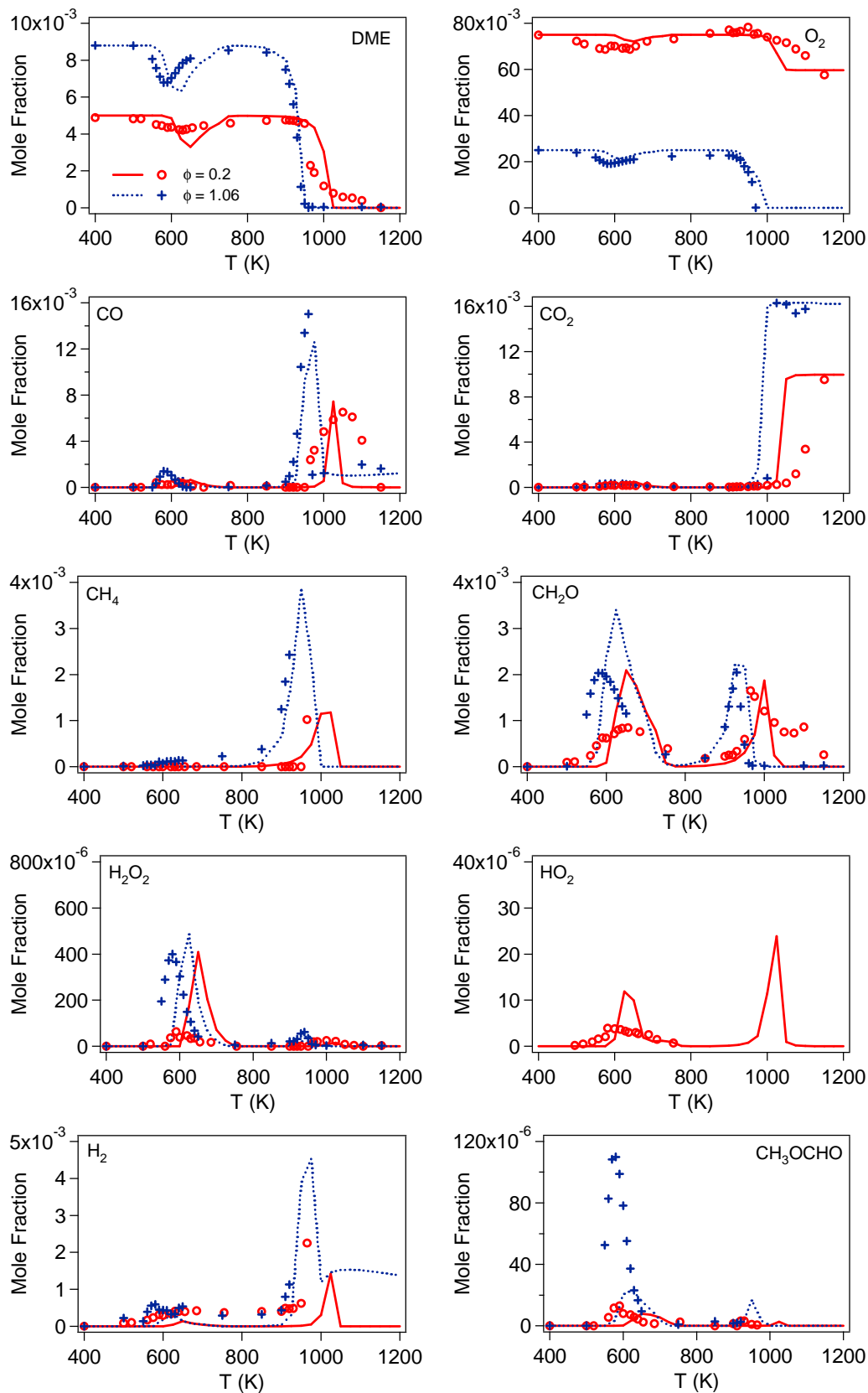


Figure 14: Comparison with flow reactor data from Kurimoto et al. [16] ($P = 1 \text{ atm}$, $\tau = 0.19 - 2.6 \text{ s}$, 5000/8800 ppm DME, 75000/25000 ppm O_2 , dilution in He/Ar). Symbols represent literature experimental data and lines the simulations using the present model.

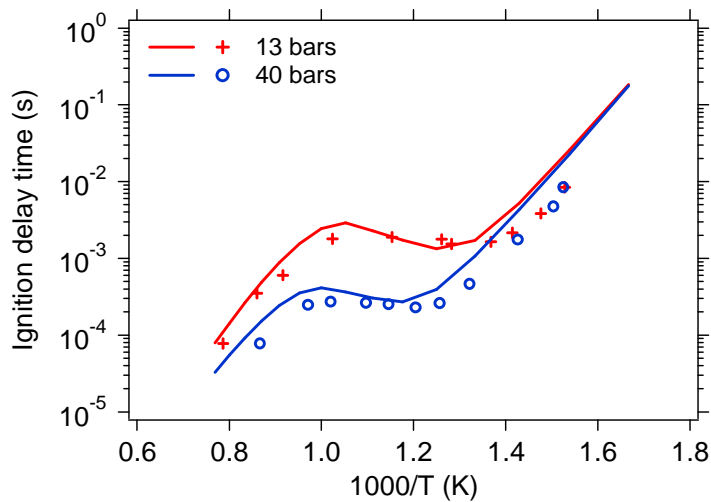


Figure 15: Comparison with shock tube data from Pfahl et al. [18] ($P = 13$ & 40 bars, stoichiometric DME/air mixtures). Symbols represent literature experimental data and lines the simulations using the present model.

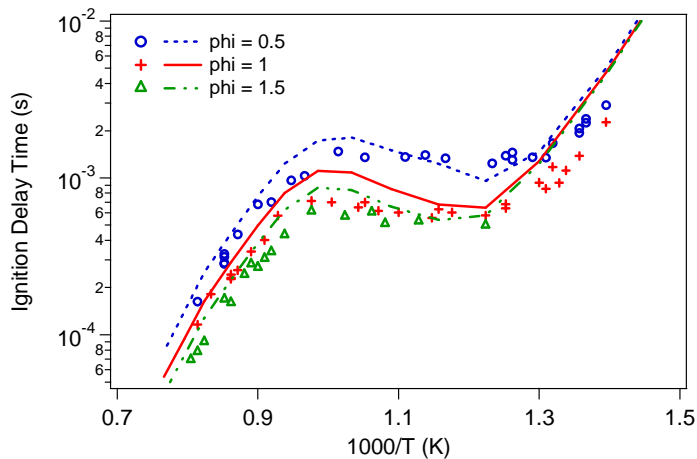


Figure 16: Comparison with shock tube data from Li et al. [19] ($P = 22$ bars, DME/air mixtures). Symbols represent literature experimental data and lines the simulations using the present model.

Rapid compression machine data obtained by Burke et al. [22] were compared with predictions using our model (Figure 17). Ignition delay times were measured at 12 and 25 bars for stoichiometric DME/air mixtures and for several equivalence ratios. Simulations were performed using the SENKIN code assuming a constant volume adiabatic reactor. Whilst this assumption has been questioned for RCM simulations where post compression volume changes may occur due to heat losses, for the shorter ignition delays simulated here this is not expected to have a major influence on the predictions as demonstrated by Serinyel et al. [81] (note that using volume history is recommended when available). Experimental data are well reproduced by simulations computed using the model developed in this study. In comparison to shock tube data previously discussed, the agreement is better and no over-estimation by the model can be observed.

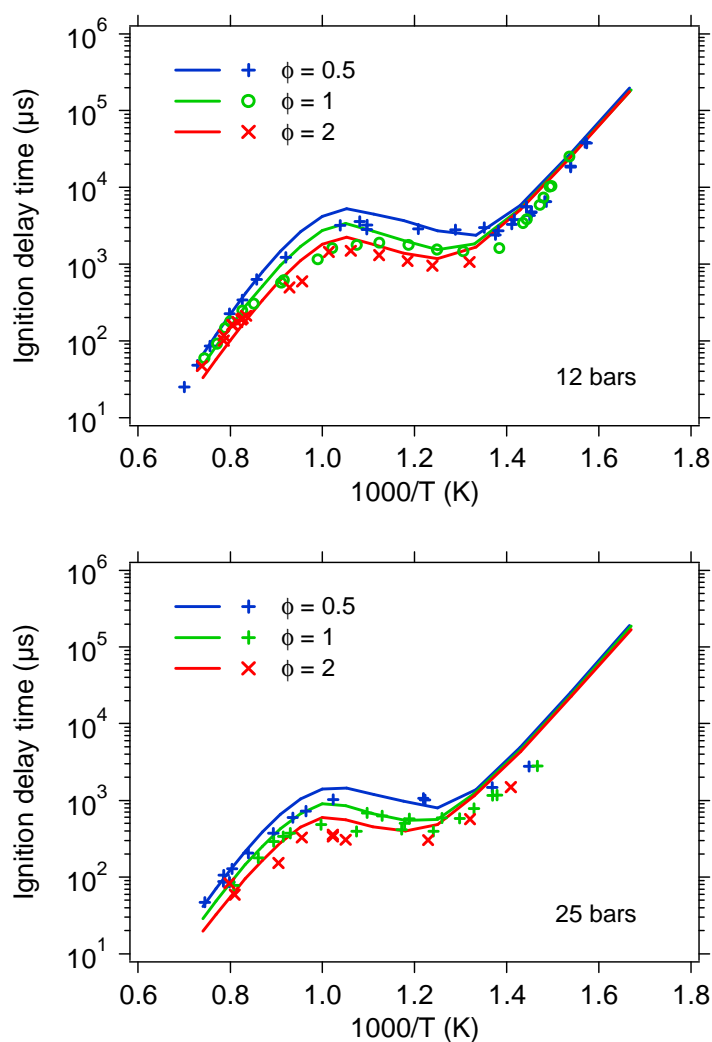


Figure 17: Comparison with RCM data from Burke et al. [22] ($P = 12$ & 25 bars, stoichiometric DME/air mixtures). $\phi = 0.5, 1$ and 2 . Symbols represent literature experimental data and lines the simulations using the present model.

The comparison with rapid compression machine data at 10 bars from Mittal et al. [21] is shown in Figure S7 in supplementary material. The studied temperature range is more limited than that in other shock tube and rapid compression machine studies. Computed ignition delay times are of the same magnitude order than experimental data. The most important deviations are observed under the richest conditions ($\phi = 1.5$) where the model does not reproduce well the negative temperature coefficient behavior.

- Flame structure comparison

A comparison was performed with low-pressure flame structure data obtained by Liu et al. [28]. The comparison is given in supplementary material (Figures S8 and S9). The agreement is remarkably good for both reactants and main reaction products (H_2 , H_2O , CO , CO_2 and CH_4 in Figure S8). Deviations are observed for formaldehyde: for this species, the formation peak is well located but computed mole fractions are over-predicted by a factor of 2 .

- Laminar burning velocity comparison

Laminar burning velocities computed using the present model were compared with the abundant data found in literature [29–35]. As stated by de Vries et al. [35], large disparities are observed between different sets of data. These disparities cannot only be attributed to slight differences in initial conditions (e.g., temperature of fresh gas, pressure). They are more likely due to procedures used for measuring laminar burning velocities with different techniques and to the nature of the fuel (e.g., adsorption phenomena before the combustion occurs). Figure 18 displays the comparison of computed and experimental laminar burning velocities under ambient conditions. Simulations were performed at 1 bar and a fresh gas temperature of 298 K. The agreement between computed and experimental data is satisfactory over the whole range of equivalence ratios. Note that the present model predicts laminar burning velocities in good agreement with the lowest experimental measurements. The maximum computed laminar burning velocity is obtained at $\varphi = 1.1$.

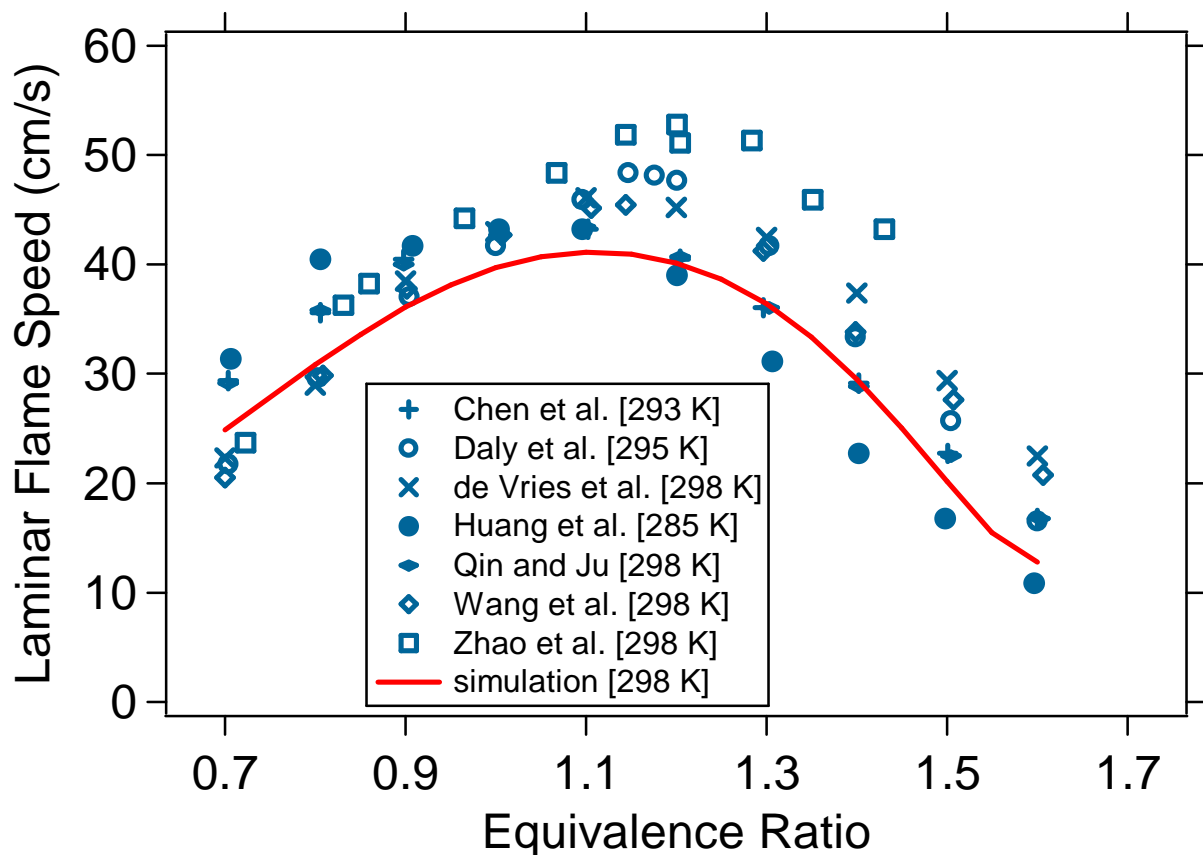


Figure 18: Comparison with laminar burning velocities from the literature ($P \approx 1$ bar, $T \approx 298$ K).

Conclusion

A study of the oxidation of dimethylether was performed using a jet-stirred reactor over the temperature range 500 – 1100 K, at a residence time of 2 s, a pressure of 106.7 kPa, at three equivalence ratios (0.25, 1 and 2) and at a constant fuel inlet mole fraction of 0.02. Reaction products exiting the reactor were quantified using gas chromatography and continuous wave cavity ring down spectroscopy. Reaction products were hydrogen (traces), water, hydrogen peroxide, C₁-C₃ hydrocarbons (methane, acetylene, ethylene, ethane, propene and propane) and C₁-C₂ oxygenated compounds (CO, CO₂, formaldehyde, acetaldehyde and methyl-formate). The experimental data obtained during this study showed that dimethylether had a significant low-temperature reactivity with a start of the reactivity observed from 500 K (an alkane of similar size like propane would not be reactive under the same conditions) and with reactivity still observed in the negative temperature coefficient zone. At low-temperature only oxygenated products were formed whereas hydrocarbons were only observed at high-temperature. At low-temperature important mole fractions of water, CO, hydrogen peroxide and formaldehyde were observed.

A new model was developed in the present study. This model is based on the high-temperature chemistry for the oxidation of DME such as that proposed in models from the literature. The reactions specific to DME oxidation at low-temperature were up-dated and coupled to the C₀-C₂ reaction base. Quantum calculations have been performed to obtain the kinetic parameters of reactions involved in the low-temperature oxidation part of the model (isomerization of RO₂• to •QOOH and reactions of •QOOH). The new model enables an improved prediction of the JSR reactivity, especially at low-temperature. Simulations using this model were also compared with experimental data from the literature covering a large range of conditions (jet-stirred reactor, flow reactor, shock tube, rapid compression machine and flame data). Overall the obtained agreement was satisfactory for the reactivity and major reaction products.

The kinetic analysis of the model developed in the present work allows a better understanding of the particular chemistry which is involved during the oxidation of DME. First the “early” reactivity observed from 500 K can easily be explained by the impossibility for the CH₃OCH₂• radical to react through inhibiting reactions “R• + O₂ = olefin + HO₂•” which competes with the first addition to O₂ during the oxidation of fuels like alkanes. Second the relative importance of the second addition to O₂ and of the reactions of decomposition of the •CH₂OCH₂OOH drives the reactivity as it defines the ratio between branching chain channels promoting the reactivity and propagation reactions which have an inhibiting effect. The important formation of hydrogen peroxide, deriving from HO₂• usually formed from oxidation reactions involving fuel radicals (non-existent here), are explained by secondary reactions of formaldehyde which is one of the main intermediates in the oxidation of dimethylether. Note that revisiting reactions of formaldehyde would likely benefit to the quality of the predictions performed using DME oxidation models.

This study showed that the presence of the oxygen atom in the fuel molecule induces important changes in the oxidation chemistry compared to that of alkanes (higher reactivity, enhanced formation of oxygenated pollutants). More investigations about the oxidation chemistry of oxygenated fuels are needed to fully understand the impact of their incorporation into conventional fuels in term of reactivity and emissions.

References

- [1] C. Arcoumanis, C. Bae, R. Crookes, E. Kinoshita, *Fuel* 87 (2008) 1014.
- [2] S. Bhattacharya, K.B. Kabir, K. Hein, *Prog. Energy Combust. Sci.* 39 (2013) 577.
- [3] M. Naqvi, J. Yan, E. Dahlquist, *Bioresour. Technol.* 101 (2010) 8001.
- [4] K. Kohse-Höinghaus, P. Oßwald, T.A. Cool, T. Kasper, N. Hansen, F. Qi, C.K. Westbrook, P.R. Westmoreland, *Angew. Chem. Int. Ed.* 49 (2010) 3545.
- [5] Z. Azizi, M. Rezaeimanesh, T. Tohidian, M.R. Rahimpour, *Chem. Eng. Process. Process Intensif.* 82 (2014) 150.
- [6] B. Prabhakar, S. Jayaraman, R. Vander Wal, A. Boehman, in: ASME, 2013, p. V002T02A021.
- [7] M.U. Alzueta, J. Muro, R. Bilbao, P. Glarborg, *Isr. J. Chem.* 39 (1999) 73.
- [8] S.L. Fischer, F.L. Dryer, H.J. Curran, *Int. J. Chem. Kinet.* 32 (2000) 713.
- [9] H.J. Curran, S.L. Fischer, F.L. Dryer, *Int. J. Chem. Kinet.* 32 (2000) 741.
- [10] I. Liu, N.W. Cant, J.H. Bromly, F.J. Barnes, P.F. Nelson, B.S. Haynes, *Chemosphere* 42 (2001) 583.
- [11] F. Herrmann, P. Oßwald, K. Kohse-Höinghaus, *Proc. Combust. Inst.* 34 (2013) 771.
- [12] F. Herrmann, B. Jochim, P. Oßwald, L. Cai, H. Pitsch, K. Kohse-Höinghaus, *Combust. Flame* 161 (2014) 384.
- [13] Z. Wang, X. Zhang, L. Xing, L. Zhang, F. Herrmann, K. Moshhammer, F. Qi, K. Kohse-Höinghaus, *Combust. Flame* (2015) doi:10.1016/j.combustflame.2014.10.003.
- [14] H. Guo, W. Sun, F.M. Haas, T. Farouk, F.L. Dryer, Y. Ju, *Proc. Combust. Inst.* 34 (2013) 573.
- [15] B. Brumfield, W. Sun, Y. Ju, G. Wysocki, *J. Phys. Chem. Lett.* 4 (2013) 872.
- [16] N. Kurimoto, B. Brumfield, X. Yang, T. Wada, P. Diévar, G. Wysocki, Y. Ju, *Proc. Combust. Inst.* 35 (2015) 457.
- [17] C. Bahrini, O. Herbinet, P.-A. Glaude, C. Schoemaeker, C. Fittschen, F. Battin-Leclerc, *J. Am. Chem. Soc.* 134 (2012) 11944.
- [18] U. Pfahl, K. Fieweger, G. Adomeit, *Proc. Combust. Inst.* 26 (1996) 781.
- [19] Z. Li, W. Wang, Z. Huang, M.A. Oehlschlaeger, *Energy Fuels* 27 (2013) 2811.
- [20] P.T. Lynch, T.P. Troy, M. Ahmed, R.S. Tranter, *Anal. Chem.* (2015) 10.1021/ac5041633.
- [21] G. Mittal, M. Chaos, C.-J. Sung, F.L. Dryer, *Fuel Process. Technol.* 89 (2008) 1244.
- [22] U. Burke, K.P. Somers, P. O'Toole, C.M. Zinner, N. Marquet, G. Bourque, E.L. Petersen, W.K. Metcalfe, Z. Serinyel, H.J. Curran, *Combust. Flame* 162 (2015) 315.
- [23] A. McIlroy, T.D. Hain, H.A. Michelsen, T.A. Cool, *Proc. Combust. Inst.* 28 (2000) 1647.
- [24] E.W. Kaiser, T.J. Wallington, M.D. Hurley, J. Platz, H.J. Curran, W.J. Pitz, C.K. Westbrook, *J. Phys. Chem. A* 104 (2000) 8194.
- [25] T.A. Cool, J. Wang, N. Hansen, P.R. Westmoreland, F.L. Dryer, Z. Zhao, A. Kazakov, T. Kasper, K. Kohse-Höinghaus, *Proc. Combust. Inst.* 31 (2007) 285.
- [26] J. Wang, U. Struckmeier, B. Yang, T.A. Cool, P. Osswald, K. Kohse-Höinghaus, T. Kasper, N. Hansen, P.R. Westmoreland, *J. Phys. Chem. A* 112 (2008) 9255.
- [27] H. Xu, C. Yao, T. Yuan, K. Zhang, H. Guo, *Combust. Flame* 158 (2011) 1673.
- [28] D. Liu, J. Santner, C. Togbé, D. Felsmann, J. Koppmann, A. Lackner, X. Yang, X. Shen, Y. Ju, K. Kohse-Höinghaus, *Combust. Flame* 160 (2013) 2654.
- [29] Z. Zhao, A. Kazakov, F.L. Dryer, *Combust. Flame* 139 (2004) 52.
- [30] Y.L. Wang, A.T. Holley, C. Ji, F.N. Egolfopoulos, T.T. Tsotsis, H.J. Curran, *Proc. Combust. Inst.* 32 (2009) 1035.
- [31] C.A. Daly, J.M. Simmie, J. Würmel, N. Djebaïli, C. Paillard, *Combust. Flame* 125 (2001) 1329.

- [32] X. Qin, Y. Ju, *Proc. Combust. Inst.* 30 (2005) 233.
- [33] Z. Huang, Q. Wang, J. Yu, Y. Zhang, K. Zeng, H. Miao, D. Jiang, *Fuel* 86 (2007) 2360.
- [34] Z. Chen, L. Wei, Z. Huang, H. Miao, X. Wang, D. Jiang, *Energy Fuels* 23 (2009) 735.
- [35] J. de Vries, W.B. Lowry, Z. Serinyel, H.J. Curran, E.L. Petersen, *Fuel* 90 (2011) 331.
- [36] P. Dagaut, J.C. Boettner, M. Cathonnet, *Symp. Int. Combust.* 26 (1996) 627.
- [37] P. Dagaut, C. Daly, J.S. Simmie, M. Cathonnet, *Symp. Int. Combust.* 27 (1998) 361.
- [38] K. Moshhammer, A.W. Jasper, D.M. Popolan-Vaida, A. Lucassen, P. Dievart, H.M. Selim, A.J. Eskola, C.A. Taatjes, S.R. Leone, M. Sarathy, Y. Ju, P. Dagaut, K. Kohse-Hoinghaus, N. Hansen, *J. Phys. Chem. A* (2015) 10.1021/acs.jpca.5b00101.
- [39] Z. Zhao, M. Chaos, A. Kazakov, F.L. Dryer, *Int. J. Chem. Kinet.* 40 (2008) 1.
- [40] R.D. Cook, D.F. Davidson, R.K. Hanson, *Proc. Combust. Inst.* 32 (2009) 189.
- [41] C. Tang, L. Wei, J. Zhang, X. Man, Z. Huang, *Energy Fuels* 26 (2012) 6720.
- [42] O. Herbinet, P.-M. Marquaire, F. Battin-Leclerc, R. Fournet, *J. Anal. Appl. Pyrolysis* 78 (2007) 419.
- [43] O. Herbinet, G. Dayma, in: F. Battin-Leclerc, J.M. Simmie, E. Blurock (Eds.), *Clean. Combust.*, Springer London, 2013, pp. 183–210.
- [44] O. Herbinet, F. Battin-Leclerc, *Int. J. Chem. Kinet.* 46 (2014) 619.
- [45] C. Bahrini, O. Herbinet, P.-A. Glaude, C. Schoemaeker, C. Fittschen, F. Battin-Leclerc, *Chem. Phys. Lett.* 534 (2012) 1.
- [46] C. Bahrini, P. Morajkar, C. Schoemaeker, O. Frottier, O. Herbinet, P.-A. Glaude, F. Battin-Leclerc, C. Fittschen, *Phys. Chem. Chem. Phys.* 15 (2013) 19686.
- [47] P. Morajkar, C. Schoemaeker, C. Fittschen, *J. Mol. Spectrosc.* 281 (2012) 18.
- [48] P. Macko, D. Romanini, S.N. Mikhailenko, O.V. Naumenko, S. Kassi, A. Jenouvrier, V.G. Tyuterev, A. Campargue, *J. Mol. Spectrosc.* 227 (2004) 90.
- [49] A.E. Parker, C. Jain, C. Schoemaeker, P. Szriftgiser, O. Votava, C. Fittschen, *Appl. Phys. B Lasers Opt.* 103 (2011) 725.
- [50] M. Cord, B. Husson, J.C. Lizardo Huerta, O. Herbinet, P.-A. Glaude, R. Fournet, B. Sirjean, F. Battin-Leclerc, M. Ruiz-Lopez, Z. Wang, M. Xie, Z. Cheng, F. Qi, *J. Phys. Chem. A* 116 (2012) 12214.
- [51] P.A. Glaude, O. Herbinet, S. Bax, J. Biet, V. Warth, F. Battin-Leclerc, *Combust. Flame* 157 (2010) 2035.
- [52] J.B. Pedley, *Thermochemical Data of Organic Compounds*, 2nd ed., Chapman and Hall, London, 1986.
- [53] R. Atkinson, D.L. Baulch, R.A. Cox, R.F. Hampson, J.A. Kerr, M.J. Rossi, J. Troe, *J. Phys. Chem. Ref. Data* 28 (1999) 191.
- [54] R.X. Fernandes, C. Fittschen, H. Hippler, *React. Kinet. Catal. Lett.* 96 (2009) 279.
- [55] D.L. Baulch, C.J. Cobos, R.A. Cox, P. Frank, G. Hayman, T. Just, J.A. Kerr, T. Murrells, M.J. Pilling, J. Troe, R.W. Walker, J. Warnatz, *J. Phys. Chem. Ref. Data* 23 (1994) 847.
- [56] C. Bansch, J. Kiecherer, M. Szöri, M. Olzmann, *J. Phys. Chem. A* 117 (2013) 8343.
- [57] R.S. Tranter, R.W. Walker, *Phys. Chem. Chem. Phys.* 3 (2001) 4722.
- [58] R.S. Tranter, P.T. Lynch, C.J. Annesley, *J. Phys. Chem. A* 116 (2012) 7287.
- [59] K. Takahashi, O. Yamamoto, T. Inomata, M. Kogoma, *Int. J. Chem. Kinet.* 39 (2007) 97.
- [60] J. Sehested, K. Sehested, J. Platz, H. Egsgaard, O.J. Nielsen, J. Sehested, K. Sehested, J. Platz, H. Egsgaard, O.J. Nielsen, *Int. J. Chem. Kinet.* 29 (1997) 627.
- [61] K. Suzuki, N. Kanno, K. Tonokura, M. Koshi, K. Tsuchiya, A. Tezaki, *Chem. Phys. Lett.* 425 (2006) 179.

- [62] C.M. Rosado-Reyes, J.S. Francisco, J.J. Szente, M.M. Maricq, L. Frøsig Østergaard, J. Phys. Chem. A 109 (2005) 10940.
- [63] D.L. Allara, R. Shaw, J. Phys. Chem. Ref. Data 9 (1980) 523.
- [64] F. Buda, R. Bounaceur, V. Warth, P.A. Glaude, R. Fournet, F. Battin-Leclerc, Combust. Flame 142 (2005) 170.
- [65] Q.S. Li, Y. Zhang, S. Zhang, J. Phys. Chem. A 108 (2004) 2014.
- [66] L.A. Curtiss, P.C. Redfern, K. Raghavachari, J. Chem. Phys. 126 (2007) 084.
- [67] M.J. Frisch, G.W. Trucks, J.R. Cheeseman, G. Scalmani, M. Caricato, H.P. Hratchian, X. Li, V. Barone, J. Bloino, G. Zheng, T. Vreven, J.A. Montgomery, G.A. Petersson, G.E. Scuseria, H.B. Schlegel, H. Nakatsuji, A.F. Izmaylov, R.L. Martin, J.L. Sonnenberg, J.E. Peralta, J.J. Heyd, E. Brothers, F. Ogliaro, M. Bearpark, M.A. Robb, B. Mennucci, K.N. Kudin, V.N. Staroverov, R. Kobayashi, J. Normand, A. Rendell, R. Gomperts, V.G. Zakrzewski, M. Hada, M. Ehara, K. Toyota, R. Fukuda, J. Hasegawa, M. Ishida, T. Nakajima, Y. Honda, O. Kitao, H. Nakai, Gaussian 09, 2009.
- [68] C. Eckart, Phys. Rev. 35 (1930) 1303.
- [69] K.S. Pitzer, W.D. Gwinn, J. Chem. Phys. 10 (1942) 428.
- [70] V. Mokrushin, W. Tsang, Chemrate v1.5.2, National Institute of Standards and Testing, Gaithersburg, USA, 2009.
- [71] A.J. Eskola, S.A. Carr, R.J. Shannon, B. Wang, M.A. Blitz, M.J. Pilling, P.W. Seakins, S.H. Robertson, J. Phys. Chem. A 118 (2014) 6773.
- [72] R.J. Kee, F.M. Rupley, J.A. Miller, Sandia Laboratories Report S 89-8009B, 1993.
- [73] A.S. Tomlin, E. Agbro, V. Nevrlý, J. Dlabka, M. Vašinek, Int. J. Chem. Kinet. 46 (2014) 662.
- [74] É. Hébrard, A.S. Tomlin, R. Bounaceur, F. Battin-Leclerc, Proc. Combust. Inst. 35 (2015) 607.
- [75] S.P. Sander, R.R. Friedl, J.R. Barker, D.M. Golden, M.J. Kurylo, P.H. Wine, J.P.D. Abbatt, J.B. Burkholder, C.E. Kolb, G.K. Moortgat, R.E. Huie, V.L. Orkin, Chemical Kinetics and Photochemical Data for Use in Atmospheric Studies, National Aeronautics and Space Administration, Jet Propulsion Laboratory California Institute of Technology Pasadena, California, 2011.
- [76] D.L. Baulch, C.T. Bowman, C.J. Cobos, R.A. Cox, T. Just, J.A. Kerr, M.J. Pilling, D. Stocker, J. Troe, W. Tsang, R.W. Walker, J. Warnatz, J. Phys. Chem. Ref. Data 34 (2005) 757.
- [77] C. Spearman, Am. J. Psychol. 15 (1904) 72.
- [78] R.S. Timonen, E. Ratajczak, D. Gutman, J. Phys. Chem. 92 (1988) 651.
- [79] W. Tsang, R.F. Hampson, J. Phys. Chem. Ref. Data 15 (1986) 1087.
- [80] D. Baulch, C. Cobos, R. Cox, C. Esser, P. Frank, T. Just, J. Kerr, M. Pilling, J. Troe, R. Walker, J. Warnatz, J. Phys. Chem. Ref. Data 21 (1992) 411.
- [81] Z. Serinyel, O. Herbinet, O. Frottier, P. Dirrenberger, V. Warth, P.A. Glaude, F. Battin-Leclerc, Combust. Flame 160 (2013) 2319.